JOURNAL OF COMPUTATIONAL PHYSICS 104, 398-417 (1993)

A Discrete Model for MHD Incorporating the Hall Term

F. KAZEMINEZHAD

Physics Department, University of California, Los Angeles

J. N. LEBOEUF

Oakridge National Laboratory, Oakridge, Tennessee

F. BRUNEL

National Research Council of Canada, Montreal, Canada

AND

J. M. DAWSON

Physics Department, University of California, Los Angeles

Received March 30, 1990; revised April 28, 1992

Medium frequency plasma behavior can be investigated using an MHD model with the addition of the Hall term to the Ohm's law. Such a model embodies some electron dynamics and can therefore be used to investigate physically more complicated processes than a conventional MHD model can. From the modeling standpoint, this model works on the ion time scale and therefore avoids the shorter electron time scale associated with a two-fluid approach. Here, we present one such model with its two as well as three-dimensional versions, test it thoroughly against the linear analytic theory, and finally present an application of the model to the study of the plasma waves generated at a solar wind cometary gas interface.

CONTENTS

INTRODUCTION

Conventional ideal magnetohydrodynamics serves as an excellent tool in investigating low frequency plasma behavior (e.g., $\omega \ll \omega_{ci}$), in which domain both the electrons and the ions can respond to an externally applied electric field and move at the $c\mathbf{E} \times \mathbf{B}/B^2$ velocity. Over distances larger than a Debye length no significant electric fields can exist in a frame of reference moving with the plasma and the electrons and the ions flow together.

The set of electrons and ions together behave mainly as a charge neutral fluid. Any magnetic fields, in the ideal case (e.g., where no resistivity or other dissipation is manifested), become frozen in the fluid and move along with it. In this domain the frequencies are mainly associated with ion inertia and magnetic restoring forces. The electrons move to maintain charge neutrality and by applying this constraint they can be eliminated from the problem.[1]

As one begins to investigate the next higher frequency domain (i.e., where $\omega \sim \omega_{ci}$), one enters a domain in which the ions start to slip across the magnetic field relative to the electrons and the electrons must move along $\mathbf{B}$ to maintain charge neutrality. Thus, as one would expect, the electron and ion fluids no longer flow together and a two-fluid treatment is required. A two-fluid approach suits ones needs. However, if the full electron dynamics are kept, the highest frequencies are the electron cyclotron and plasma frequencies and one is obliged to use correspondingly short time scales; this would limit one to very short time simulations.

It turns out, however, that many important results of the two-fluid model can be obtained from a zero mass electron approximation in which the electrons are always in force balance (no electron oscillations). To achieve this, one must add the Hall term to Ohm's law. Therefore, many important

[1] Electron motion along the magnetic field can be important here.

0021-9991/93 $5.00

effects in the second frequency domain (i.e., $\omega \sim \omega_{ci}$) can be investigated using an MHD code with the addition of a single term, keeping the luxury of long time steps.

Physically the Hall term accounts for the relative slippage of the ions with respect the electrons across the magnetic field as will be proven shortly. Closed current paths ($\nabla \cdot \mathbf{j} \simeq 0$) are maintained by ion flow across **B** and electron flow along **B**. Thus, addition of the Hall term alone in an MHD code will partially allow the electrons and the ions to flow separately while the plasma remains quasi-neutral. This greatly enriches the physics by introducing new modes of oscillation.

For our urpose, a particle fluid code has been developed; i.e., a code which treats elements of the fluid as particles and follows their motion. The numerical techniques are a combination of particle simulation techniques (e.g., particle in the cell method) and fluid simulation methods (e.g., the Lax–Wendroff algorithm commonly employed in solving fluid type equations[2] for advancing **B**) [1]. Two- and three-dimensional versions of the code have been constructed. The present work represents extension of the earlier work done by Leboeuf *et al.*, Tajima *et al.*, and Brunel *et al.* [1–3].

The code has the flexibility of being used as a pure MHD code by turning off the Hall term. It can also be easily generalized to incorporate more physics by the inclusion of resistivity, and thermal transport and also multiple ion fluids can be introduced.

One technical difficulty can arise under some circumstances in using such a code to model a fluid. Fluid elements should not flow through each other; in the model two fluid elements with quite different velocities can find themselves in the same spatial grid cell (such a problem is called multi-streaming). Using a particle fluid code to model effects such as shocks in which rapid velocity changes occur within very small distances will lead to this situation. In a real gas (or plasma) such multi-streaming also tends to arise for shock situations but is prevented by viscosity (collisions). We emulate nature in the code by introducing a flexible artificial viscosity which acts as a drag between fluid elements in a given grid cell and brings the fluid elements rapidly to the same velocity.

A final remark regarding the correspondence between this approach and a pure hydrocode is in order. Here, instead of discretizing the analytic equations which form the basis of the model (i.e., the ion momentum and Faraday's law) directly, the unconventional technique of emulating fluid elements by finite-sized particles have been implemented. To a conscientious observer, this technique may appear a rather empirical one. As regards to the validity of the approach, first, averaging the particle quantities in grid cells by an interpolation scheme has the net effect of producing the pure hydrodynamic quantities of density and velocity in agreement with the later's results as will be demonstrated; second, we will show that over the frequency range where the inclusion of the Hall term has a marked effect on wave propagation properties, this approach accurately accounts for the physics as expected analytically. As regards to its usefulness, the model provides local (particle properties, e.g., trajectories and phase space) as well as global (fluid properties, e.g., averaged per cell particle quantities) information about physical problems and, in that, it stands unique. Furthermore, the finite particle temperatures provides adequate background noise needed to excite the highly dispersive waves. As one example the simulation of the solar wind cometary plasma interaction has been performed; the results show the generation of a shock region in a cometary gas solar wind interaction region with detailed depictions of particle trajectories and phase space plots. Some of these results are discussed in the application section, while others have been discussed elsewhere [4, 17]. The shock and the magnetoacoustic waves generation in the cited example agree with the MHD predictions, while the detailed particle trajectories and phase space plots which reveal vital information about the cometary particle pickup by the solar wind, the solar wind particle reflection at the shock front, etc. are only attributed to the particle aspect of the model.

The organization of the paper is as follows: in Section 1 the model is treated analytically and a dispersion relation is obtained; in Section 2 the numerical model is extensively discussed; in Section 3 we present extensive tests of the model we developed by checking that it gives the proper waves and dispersion as was obtained from the analytic treatment of the fluid equations.[3]

1. ANALYTIC TREATMENT

Using linear analytic theory as in Tajima *et al.* [2], we derive a general dispersion relation involving arbitrary angles of propagation. The starting equations will be the fluid equations and Maxwell's equations. The ion fluid momentum equation is written in a Lagrangian form (i.e., a system which moves with the fluid since fluid elements are treated like particles). The equation of motion is

$$n_i M_i \frac{d\mathbf{v}_i}{dt} = n_i e \left(\mathbf{E} + \frac{\mathbf{v}_i \times \mathbf{B}}{c} \right) - \nabla \cdot \mathbf{\Pi}_i. \tag{1}$$

Here **E** and **B** are the self-consistent electric and magnetic fields at a given point in the plasma, $\mathbf{v}_i$ is the ion fluid velocity, $\mathbf{\Pi}_i$ is the ion pressure tensor, and, finally, n_i is the ion density at that point.

[2] That is, equations which involve advective terms.

[3] We have also shown that the model gives shocks with the proper jump condition [4].

Likewise the electron fluid momentum equation is

$$n_e m_e \frac{d\mathbf{v}_e}{dt} = -n_e e\left(\mathbf{E} + \frac{\mathbf{v}_e \times \mathbf{B}}{c}\right) - \nabla \cdot \mathbf{\Pi}_e \cong 0, \tag{2}$$

where the last $\cong 0$ holds for m_e set equal to zero. By assuming the electron to have zero mass, since we are interested in low frequencies, and neglecting electron pressure, Eq. (2) gives the following for the electric field **E**:

$$\mathbf{E} = -\frac{\mathbf{v}_e \times \mathbf{B}}{c}. \tag{3}$$

This is identical to the assumption of perfect conductivity along the magnetic field (a useful approximation for many plasmas of interest) and yields

$$\mathbf{E} \cdot \mathbf{B} = 0. \tag{4}$$

These assumptions can be relaxed and resistivity and electron pressure can be included; of course, this requires that Eq. (4) be modified.

The equations for conservation of ions and electrons are given by Eq. (5):

$$\frac{dn_{i,e}}{dt} = \frac{\partial n_{i,e}}{\partial t} + \nabla \cdot (n_{i,e}\mathbf{v}_{i,e}) = 0. \tag{5}$$

As already explained for low frequency modes we assume quasi-neutrality $n_i \cong n_e \cong n$ (here $\cong$ means equal to a very high degree; we use $=$ from now on). Charge neutrality requires that the current is divergence-free; i.e.,

$$\nabla \cdot \mathbf{j} = 0. \tag{6}$$

Of course, the current is simply given by

$$\mathbf{j} = ne(\mathbf{v}_i - \mathbf{v}_e). \tag{7}$$

It should be noted that $n_i \cong n_e$ does not mean $\nabla \cdot \mathbf{E} = 0$, since even a very small charge imbalance leads to large **E**; the **E** that results is just what is required to give $\nabla \cdot \mathbf{j} = 0$.

These equations must be supplemented by Maxwell's equations; we omit the displacement current:

$$\nabla \times \mathbf{B} = \frac{4\pi}{c}\mathbf{j} \tag{8}$$

$$\nabla \times \mathbf{E} = \frac{-1}{c}\frac{\partial \mathbf{B}}{\partial t}. \tag{9}$$

Substituting **E** from Eq. (3) into the ion momentum, Eq. (1), results in

$$nM_i \frac{d\mathbf{v}_i}{dt} = \frac{ne(\mathbf{v}_i - \mathbf{v}_e) \times \mathbf{B}}{c} - \nabla \cdot (\mathbf{\Pi}_i). \tag{10}$$

Next, substituting **j** from Eq. (7) into this equation gives

$$nM_i \frac{d\mathbf{v}_i}{dt} = \frac{\mathbf{j} \times \mathbf{B}}{c} - \nabla \cdot (\mathbf{\Pi}_i). \tag{11}$$

Substituting for the current **j** from Ampere's law, (Eq. 8), gives

$$\rho \frac{d\mathbf{v}_i}{dt} = -\frac{\mathbf{B} \times (\nabla \times \mathbf{B})}{4\pi} - \nabla \cdot (\mathbf{\Pi}_i), \tag{12}$$

where ρ is simply the ion mass density. Next substituting for **E** from Eq. (3) into Faraday's law, (Eq. 9), after using Eqs. (7) and (8) results in the following equation for the evolution of the magnetic field:

$$\frac{\partial \mathbf{B}}{\partial t} = c\nabla \times \left[\frac{1}{c}\mathbf{v}_i \times \mathbf{B} + \frac{1}{4\pi ne}\mathbf{B} \times (\nabla \times \mathbf{B})\right]. \tag{13}$$

These last two equations (12) and (13), form the basis of our model. There are a couple of important points about Eq. (13). The first being that this equation is similar to the magnetic field evolution equation for one fluid ideal MHD, except for the presence of the second term (Hall term) on the right-hand side. The second important point is that, using Faraday's law, Eq. (9), and the current, Eq. (7), the electron fluid velocity $\mathbf{v}_e$ can be written as

$$\mathbf{v}_e = \mathbf{v}_i - \frac{c}{4\pi ne}\nabla \times \mathbf{B}. \tag{14}$$

This is simply the first two terms in Eq. (13) before the cross product with **B**; i.e., the magnetic field evolution equation is simply (neglecting the electron pressure term)

$$\frac{\partial \mathbf{B}}{\partial t} = \nabla \times (\mathbf{v}_e \times \mathbf{B}). \tag{15}$$

This now is identical to the magnetic field evolution equation for ideal MHD, except that it involves the electron fluid velocity instead of the fluid mass velocity. This means that the magnetic field is frozen to the flow of the electrons rather than to the total fluid; the ions, because of their inertia, slip with respect to **B**.

We shall next derive a dispersion relation for general (oblique) wave propagation using Eqs. (12) and (13), and the equations of continuity and state for the ions.

At first we assume that the pressure is isotropic. This being so, one obtains $\mathbf{\Pi}_i = p_i \,\underline{\underline{||}}$, where $\underline{\underline{||}}$ is the unit dyadic tensor; therefore, $\nabla \cdot (\mathbf{\Pi}_i) = \nabla p_i$ in Eq. (12). Furthermore, using an adiabatic equation of state for the ions results in

$$\nabla p_i = \gamma T_i \nabla\, \delta n_i. \tag{16}$$

Next linearizing Eqs. (12) and (13) about a spatially

uniform equilibrium,[4] we obtain the following set (we drop the subscript i):

$$\rho_0 \frac{d\mathbf{v}}{dt} = -\frac{1}{4\pi}\mathbf{B}_0 \times (\nabla \times \delta\mathbf{B}) - \gamma T \nabla \delta n \tag{17}$$

$$\frac{\partial \delta \mathbf{B}}{\partial t} = \nabla \times (\mathbf{v} \times \mathbf{B}_0) + \frac{c}{4\pi n_0 e}\nabla \times (\mathbf{B}_0 \times (\nabla \times \delta\mathbf{B})). \tag{18}$$

Assuming simple plane wave solutions. Eqs. (17) and (18) reduce to the set,

$$\rho_0(-i\omega\mathbf{v}) = -\frac{1}{4\pi}\mathbf{B}_0 \times (i\mathbf{k} \times \delta\mathbf{B}) - (\gamma T\, \delta n)\, i\mathbf{k} \tag{19}$$

$$-i\omega\, \delta\mathbf{B} = i\mathbf{k} \times (\mathbf{v} \times \mathbf{B}_0) + \bar{\alpha} i\mathbf{k} \times (\mathbf{B}_0 \times (i\mathbf{k} \times \delta\mathbf{B})); \tag{20}$$

please note that $\bar{\alpha}$ in Eq. (20) is $c/4\pi n_0 e$.

One needs to relate the densities and fluid velocities in Eqs. (19) and (20) in order to obtain the dispersion relation. This is done with the help ofthe continuity Eq. (5), which upon linearization and use of plane wave solutions gives

$$-i\omega\, \delta n_i + i n_0 \mathbf{k} \cdot \mathbf{v} = 0. \tag{21}$$

Plugging this into Eqs. (19) and (20) and substituting $\rho_0 = n_0 M$ and $c_s^2 = \gamma T_i / M$ (the ion acoustic speed), along with the repeated use of the BAC-CAB vector identity rule, gives

$$\mathbf{v} = \frac{1}{4\pi n_0 M\omega}[\mathbf{k}(\mathbf{B}_0 \cdot \delta\mathbf{B}) - \delta\mathbf{B}(\mathbf{k} \cdot \mathbf{B}_0)] + \frac{c_s^2}{\omega^2}(\mathbf{k} \cdot \mathbf{v})\mathbf{k} \tag{22}$$

$$-i\omega\, \delta\mathbf{B} = i[\mathbf{v}(\mathbf{k} \cdot \mathbf{B}_0) - \mathbf{B}_0(\mathbf{k} \cdot \mathbf{v})] + \bar{\alpha}(\mathbf{k} \cdot \mathbf{B}_0)(\mathbf{k} \times \delta\mathbf{B}). \tag{23}$$

Interestingly enough, when Eq. (23) is dotted with $\mathbf{k}$, one obtains $\mathbf{k} \cdot \delta\mathbf{B} = 0$, as should be, since $\nabla \cdot \mathbf{B} = 0$. In order to eliminate $\mathbf{v}$ from Eq. (23), let us take the dot product of Eq. (22) with $\mathbf{k}$, and use the fact that $\mathbf{k} \cdot \delta\mathbf{B} = 0$ to obtain

$$\mathbf{k} \cdot \mathbf{v} = \frac{k^2}{4\pi\rho_0\omega}\frac{\mathbf{B}_0 \cdot \delta\mathbf{B}}{(1 - k^2 c_s^2/\omega^2)} \tag{24}$$

Substituting Eq. (24) into Eq. (22) gives $\mathbf{v}$ in terms of $\delta\mathbf{B}$:

$$\mathbf{v} = \frac{1}{4\pi\rho_0\omega}[\mathbf{k}(\mathbf{B}_0 \cdot \delta\mathbf{B}) - \delta\mathbf{B}(\mathbf{k} \cdot \mathbf{B}_0)] + \frac{k^2 c_s^2}{4\pi\rho_0\omega^3}\frac{(\mathbf{B}_0 \cdot \delta\mathbf{B})\mathbf{k}}{(1 - k^2 c_s^2/\omega^2)}. \tag{25}$$

[4] The quantities with the subscript zero are the equilibrium quantities, and those preceded by δ are the perturbed ones.

Finally using Eqs. (24) and (25) in Eq. (23) results in an equation which involves only $\delta\mathbf{B}$, which can then be used to determine the dispersion relation between ω and $\mathbf{k}$; i.e.,

$$-i\omega\, \delta\mathbf{B} = i\left\{\frac{\mathbf{k} \cdot \mathbf{B}_0}{4\pi\rho_0\omega}[\mathbf{k}(\mathbf{B}_0 \cdot \delta\mathbf{B}) - \delta\mathbf{B}(\mathbf{k} \cdot \mathbf{B}_0)] + \frac{[(\mathbf{k} \cdot \mathbf{B}_0)(k^2 c_s^2/\omega^2)\mathbf{k} - \mathbf{k}^2\mathbf{B}_0](\mathbf{B}_0 \cdot \delta\mathbf{B})}{4\pi\rho_0\omega(1 - k^2 c_s^2/\omega^2)}\right\} + \bar{\alpha}(\mathbf{k} \times \delta\mathbf{B})(\mathbf{k} \cdot \mathbf{B}_0). \tag{26}$$

From this equation the dispersion relation for any angle of propagation can be obtained.

Studies of oblique waves are of particular importance. Aside from the applications to real experimental situations which will become evident in the application section, Section 4, oblique waves serve as excellent probes for testing the validity of the particle MHD code that we have developed. The reason can best be seen by looking at Fig. 1. Figure 1 shows the current flow for a general oblique wave $[\mathbf{k} = (k_{\|}, \mathbf{k}_{\perp})]$. The electron current flows parallel to $\mathbf{B}_0$; at distances separated by half a wavelength, $(\pi/k_{\perp})$, the flow is in opposite directions. Ions, however, due to their inertia, can move perpendicular to $\mathbf{B}_0$; they flow in opposite directions at distances separated by $(\pi/k_{\|})$, parallel to $\mathbf{B}_0$. The combined electron and ion currents form closed current loops so that $\nabla \cdot \mathbf{j} = 0$. The requirement that $E_{\|}$ be zero (from Eq. (4)) means that an electrostatic field develops so that its parallel component just cancels the parallel component of the inductive E.

The exact closure of the current loops, particularly for nearly perpendicular propagation, provides a severe test of a computer code; if the code gives the right dispersion relation for such waves, we can have confidence it is treating the physics correctly.

Using Eq. (26) the dispersion relation for oblique waves is obtained with $\mathbf{B}_0$ in a fixed direction; e.g., along the z axis.

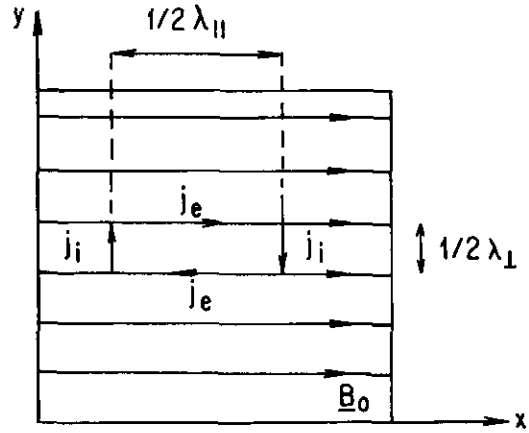

FIG. 1. Plasma response to oblique waves.

That is,

$$\omega^6+\omega^4\left\{-k^2c_s^2-(k_\perp^2+2k_{||}^2)\,c_A^2-\frac{c_A^4}{\omega_{ci}^2}k^2k_{||}^2\right\}$$
$$+\omega^2\left\{(2k_{||}^2c_s^2c_A^2+k_{||}^2c_A^4)\,k^2+\frac{c_A^4}{\omega_{ci}^2}k^4k_{||}^2c_s^2\right\}$$
$$-k^2k_{||}^4c_A^4c_s^2=0, \tag{27}$$

where the substitutions $\bar{\alpha}\mathbf{B}_0=c_A^2/\omega_{ci}$ and $c_A^2=B_0^2/4\pi\rho_0$ have been made, with c_A being the Alfven speed and $\bar{\alpha}=c/4\pi en_0$.

Next we test Eq. (27) in the limits of perpendicular and parallel propagation, respectively. For perpendicular propagation with $k_{||}=0$ the dispersion relation, Eq. (27), immediately reduces to $\omega^6+\omega^4(-k_\perp^2(c_s^2+c_A^2))=0$, which is simply the dispersion relation for magnetoacoustic waves as expected; there are also two zero-frequency modes. One of these is the zero-frequency convective mode which corresponds to simple shear flow or vortex motion and, the other zero-frequency mode corresponds to different densities being loaded on different flux tubes. For the parallel case, on the other hand, with $k_\perp=0$; Eq. 27 reduces to

$$\omega^6+\omega^4\left\{-k_{||}^2c_s^2-c_A^2\left[2k_{||}^2+\frac{c_A^2}{\omega_{ci}^2}k_{||}^4\right]\right\}$$
$$+\omega^2\left\{2k_{||}^4c_A^2c_s^2+k_{||}^4c_A^4+\frac{c_A^4}{\omega_{ci}^2}k_{||}^6c_s^2\right\}$$
$$-k_{||}^6c_A^4c_s^2=0. \tag{28}$$

This relationship gives rise to a biquadratic in the case of $c_s=0$ which has the solution

$$\omega=\pm\left[\frac{k_{||}^2c_A^2}{2\omega_{ci}}\pm k_{||}c_A\sqrt{1+\frac{k_{||}^2c_A^2}{4\omega_{ci}^2}}\right]. \tag{29}$$

This is simply the result which was obtained by Tajima *et al.* [2] for parallel propagation; it gives the whistler (right-handed) and the ion cyclotron (left-handed) waves.

For the simulation results presented in this paper, however, we required a more general dispersion relation than Eq. (27). We used Eq. (26) with $\mathbf{B}_0$ pointing at an arbitrary direction, specified by polar and azimuthal angles for comparisons with the simulation results. The interested reader is referred to Eq. (103) in Appendix A for its derivation. Equation (103) can be obtained from Eq. (27) by a simple rotation of the coordinate system. There are a couple of points about Eq. (103) and the way it has been derived. First, the reason why both the wave vector $\mathbf{k}$ and the applied magnetic field $\mathbf{B}_0$ had to be set in arbitrary directions is that, when doing simulations, arbitrary directions for both are generally encountered; in the simulations, fast Fourier transform techniques have been used which restrict $\mathbf{k}$ to discrete values. As a result, if one were to study a certain arbitrary direction for wave propagation, one needs to also change the direction of $\mathbf{B}_0$. As we shall see later, many oblique wave modes were studied and compared with this analytic disperion relation; this relation thus proved to be very useful. The second point is that this relationship, despite of its complex appearance, can be evaluated quickly numerically. We shall use Eq. (103) a great deal later for testing our model, and in our application section for determining the kinds of MHD waves that are generated in the simulation of cometary gas solar wind interactions.

2. NUMERICAL ALGORITHM

Our model is simply an intuitive construct based on well-known fluid dynamics and Maxwell's equations, geared toward plasma physics applications, where many different wave modes exist and are almost all fairly dispersive. Its physical "conceptual basis" can be regarded as a model which emulates motions with scales that are large compared to the mesh (ion collisionless skin depth) or particle size, in which the combined ion-electron dynamics adds more waves to the system than a conventional MHD model has and all of which tend to be fairly dispersive. It is this type of the phenomenon that the model attempts to address; i.e., a physical domain in which conventional MHD as well as hydrodynamic methods seem inadequate to account for the complex physical behavior caused by the multitude of waves and their dispersion.

We mathematically treat the fluid as an ensemble of discrete elements or "particles"; i.e., we have divided the fluid into small (but finite elements) which we treat as "particles" and push them around in accordance with the magnetic and pressure forces they experience; i.e., quasi-particles whose orbits follow closely the motion of fluid elements although they cannot stretch and deform like real fluid elements. Real fluids are made of molecules and atoms (many more than we use) which are locally locked together by collisions. These "particles" can be followed and this is what our model does.

Equations (12) and (13) form the basis of the model. The model employs a combination of Lagrangian and Eulerian schemes; i.e., Lagrangian for the fluid elements and Eulerian for the field equations. Equation (12) is a well-known equation of fluid dynamics and describes how an infinitesimal element of the fluid moves. It is identical to Eq. (6.44) in Potter [7] for the more simplified case of pure hydrodynamic flow.

In the course of following the motion of "particles" two or more elements can occupy the same region of space (the same spatial grid). To a large extent, this is inhibited by pressure and magnetic forces, but it does happen, particularly if there are more "particles" than cells. The fact

that two or more "particles" can occupy the same cell necessitates the introduction of $\mathbf{v}_f$, the mean ion fluid velocity. The **B** field motion is controlled by the electron motion which responds to the total ion motion, i.e., $\mathbf{v}_f$, and the velocity of an individual fluid element. The grid we use in solving the field equations is fixed in space and does not move with the fluid and, hence, cannot become tangled up due to the fluid vortex motion. Furthermore, the presence of two or more "particles" in the same cell will mean collisions. In a real fluid there are many molecules in a very small volume of the fluid which we can consider a fluid element. They are strongly locked together in their motion by collisions. That is what the viscous drag between particles in the same cell does in our model; i.e., an absorption mechanism is provided by the strong drag between particles with different velocities in one cell.

To sum up, "particle" positions are initialized on a fixed background mesh; Eq. (12) is used to accelerate the "particles" in their self-consistent magnetic and pressure forces, using a Lagrangian scheme (leapfrog scheme); the fluid density, velocity, and pressure are computed by an interpolation scheme as weighted averages of the particles' quantities on the given spatial grids; the magnetic field is then pushed, using the interpolated velocity $\mathbf{v}_f$ in Eq. (13) by an Eulerian approach (a Lax–Wendroff method is used). This then completes a full cycle of calculations. The remainder of this section is devoted to the details of these steps.

2.1. *Normalization*

In these calculations we use the following normalization. All the velocities in Eqs. (12) and (13) are normalized to the ion acoustic speed c_s, the magnetic field to the ratio of the Alfven speed to the ion acoustic speed, all the spatial distances are normalized to the grid size, Δ, and the time to the time that it takes an ion acoustic wave to travel one grid space. All of these remarks can be summarized as

$$\tilde{\mathbf{B}} = \frac{\mathbf{B}}{\sqrt{4\pi\rho_0}\, c_s}, \qquad \nabla = \frac{1}{\Delta}\tilde{\nabla} \tag{30}$$

$$\frac{\partial}{\partial t} = \frac{c_s}{\Delta}\frac{\partial}{\partial \tilde{t}}, \qquad \tilde{\mathbf{v}} = \frac{\mathbf{v}}{c_s}, \tag{31}$$

where the quantities with the tilde are the normalized quantities used in the code.

An adiabatic equation of state was used for the ions; i.e., $p_i/\rho^\gamma = \text{const}$; only an ion pressure was used. Upon introducing the above, Eqs. (12) and (13) in their normalized form are

$$\frac{d\mathbf{v}}{dt} = \frac{n_0}{n}(\nabla \times \mathbf{B}) \times \mathbf{B} - \frac{1}{n}\left(\frac{n}{n_0}\right)^{\gamma - 1} \nabla n \tag{32}$$

$$\frac{\partial \mathbf{B}}{\partial t} = \nabla \times \left\{ \mathbf{v}_f \times \mathbf{B} - \frac{\lambda}{\Delta}\frac{n_0}{n}(\nabla \times \mathbf{B}) \times \mathbf{B} \right\}. \tag{33}$$

The tildes have been dropped here for simplicity. Furthermore, the $\mathbf{v}$ which appears in Eq. (32) is that of fluid particles, while the $\mathbf{v}_f$ which appears in Eq. (33) is the average fluid velocity of all particles in a given grid cell. Furthermore in Eq. (33), the Hall term is simply the coefficient λ/Δ, where λ is the collisionless skin depth for ions; i.e., $\lambda = c/\omega_{pi}$ (here $\Delta = 1\lambda$).[5] It should now be clear that Eq. (33) is just like the MHD equation for the magnetic field induction except for the presence of the second term on the right-hand side, the Hall term. One interesting feature of Eq. (33) can be readily seen, namely, that if one sets $\lambda = 0$, then one obtains the ideal MHD equation for the magnetic field evolution. Thus the code has the flexibility of being easily converted to a standard MHD one and tested.

2.2. *The Numerical Scheme*

Next we shall describe the numerical scheme. The steps of the scheme are summarized in Table I. A leapfrog scheme is used to push the particles for Eq. (32), while a Lax–Wendroff method is used to push **B** for Eq. (33); these have been implemented as follows.

The particle positions $\mathbf{r}_i$, the density n, and the pressure p and **B** are known at integer time steps l; the particle velocities $\mathbf{v}$ are known at half-integer time steps $1 \pm \frac{1}{2}$ as illustrated in Fig. 2.

First, $\mathbf{v}$ is pushed a half time step from time step $l - \frac{1}{2}$ to the time step l using Eq. (32) and the values of **B** and p at time step l. Next, **B** is pushed from l to $l + \frac{1}{2}$ as the auxiliary step of the Lax–Wendroff scheme using Eq. (33) with the spatial average values of **B** (please refer to item 5 of the Table I) and the fluid velocity[6] $\mathbf{v}_f$ at time step l. Then again the fluid particle velocities are pushed from time step l to $l + \frac{1}{2}$, using the values of **B** and p at the time step l in Eq. (32). Having known $\mathbf{v}_f$ and **B** at time step $l + \frac{1}{2}$, we push **B** all the way to time step $l + 1$ as the main step of the Lax–Wendroff scheme in Eq. (32).

To avoid multi-streaming of fluid elements, an artificial drag (artificial viscosity) between particles in a single grid cell is included with a variable coefficient f which can be adjusted to any desired value. The method of adding adjustable artificial viscosity terms to handle steep gradients and inviscid shocks were initially used by Von Neumann [5]. Leboeuf *et al.* [1] also used this technique for studying shocks using a one-dimensional model. Here the artificial viscosity is introduced as a force which tends to drag particle velocities to the average of the velocity of all particles in its grid cell. This is accomplished by dragging the ith particle's velocity by

$$\Delta \mathbf{v}_i = f\left\{ \mathbf{v}_i - \frac{\sum_{j \in \Delta_i} \mathbf{v}_j}{\sum_{j \in \Delta_i} n_j} \right\} \tag{34}$$

[5] Choosing $\Delta \neq 1\lambda$ corresponds to taking grid spacings not the same as the skin depth.

[6] Obtained from the area-weighting interpolation scheme that will be discussed shortly.

TABLE I

Numerical Algorithm of the MHD Hall Term Model

Initially we have: $\mathbf{B}^l$, $\mathbf{v}^{l-1/2}$, $\mathbf{r}^l$

1. Compute fluid density n^l from particle positions by interpolation.
2. Compute magnetic and pressure forces: $[(\nabla\times\mathbf{B})\times\mathbf{B}=-\nabla\cdot((B^2/2)\,\bar{\bar{I}}-\mathbf{BB})]$

$$\mathbf{F}_B^l=\frac{n_0}{n^l}\left[-\nabla\cdot\left(\frac{B^2}{2}\,\bar{\bar{I}}-\mathbf{BB}\right)\right]^l,$$

$$\mathbf{F}_p^l=-\frac{1}{n^l}\left(\frac{n^l}{n_0}\right)^{\gamma-1}\nabla n$$

$$\mathbf{F}^l=\mathbf{F}_p^l+\mathbf{F}_B^l.$$

3. Push velocities half a time step:

$$\mathbf{v}^l=\mathbf{v}^{l-1/2}+\mathbf{F}^l\,\Delta t/2.$$

4. Compute fluid velocoties $\mathbf{v}_f^l$ from particle velocities by interpolation.
5. Push $\mathbf{B}$ half a time step as the auxiliary step of the Lax–Wendroff scheme:

$$\mathbf{B}^{l+1/2}=\langle\mathbf{B}\rangle^l+\left(\nabla\times\left[\mathbf{v}_f^l\times\mathbf{B}^l+\lambda\frac{n_0}{n^l}\nabla\cdot\left(\frac{B^2}{2}\,\bar{\bar{I}}-\mathbf{BB}\right)^l\right]\right)\Delta t/2,$$

where $\langle\mathbf{B}\rangle_{ij}^n=\frac{1}{4}(B_{i+1,j}^n+B_{i-1,j}^n+B_{i,j+1}^n+B_{i,j-1}^n)$ in two dimensions and in three dimensions $\langle\mathbf{B}\rangle_{i,j,k}$ has been properly averaged using the edges of a cube surrounding the grid point $\{i,j,k\}$.

6. Push the velocities another half a time step:

$$\mathbf{v}^{l+1/2}=\mathbf{v}^l+\mathbf{F}^l\,\Delta t/2+f(\mathbf{v}_f^l-\mathbf{v}^l);$$

clearly then for $f=0$, $\mathbf{v}^{l+1/2}=\mathbf{v}^{l-1/2}+\mathbf{F}^l\,\Delta t\Rightarrow$ we have a leap frog for $\mathbf{v}$.

7. Push positions half a time step:

$$\mathbf{r}^{l+1/2}=\mathbf{r}^l+\mathbf{v}^{l+1/2}\,\Delta t/2.$$

8. Compute fluid velocities $\mathbf{v}_f^{l+1/2}$ by interpolation.
9. Push $\mathbf{B}$ a full time step as the main step of the Lax–Wendroff scheme:

$$\mathbf{B}^{l+1}=\mathbf{B}^l+\left(\nabla\times\left[\mathbf{v}_f^{l+1/2}\times\mathbf{B}^{l+1/2}+\lambda\frac{n_0}{n^{l+1/2}}\nabla\cdot\left(\frac{B^2}{2}\,\bar{\bar{I}}-\mathbf{BB}\right)^{l+1/2}\right]\right)\Delta t.$$

10. Push positions half a time step: $\mathbf{r}^{l+1}=\mathbf{r}^{l+1/2}+\mathbf{v}^{l+1/2}\,\Delta t/2$. Clearly here also, $\mathbf{r}^{l+1}=\mathbf{r}^l+\mathbf{v}^{l+1/2}\,\Delta t\Rightarrow$ a leapfrog for $\mathbf{r}$.

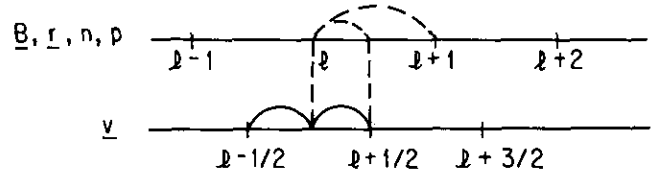

FIG. 2. Time stepping scheme for $\mathbf{B}$, $\mathbf{r}$, n, p, $\mathbf{v}$.

per time step. Here the sum over all j is over all the particles in the same cell as particle i[7]; f is chosen between 0 and 1; 0 gives no viscosity while 1 gives instant velocity relaxation to the average. This completes a full cycle of a time step. Table I summarizes this.

2.3. *Interpolation Scheme*

Particles are given a finite size in order to smooth out density variations and to offset the need for a large number of particles. Also since a discrete grid is used, there is a minimum resolvable size for a disturbance and so our particles (fluid elements) might as well also be of this size. In this code, however, the spatial extent simply gives rise ro a mass distribution about the center of the particles.

The method of interpolation used in this code is a simple area-weighting method which is extensively discussed by Birdsall *et al.* [6]. Using those techniques in one dimension for the finite sized particles of size a ($\Delta\leqslant a\leqslant 2\Delta$), i.e., particles which can overlap at the most three grid cells at a time, the weight function $w(x)$ as seen by the grid point x_j due to a particle at a distance x streaming from left to right is found to be

$$w(x)=\begin{cases}\dfrac{x+\Delta ax}{a}, & x\in\left(x_j-\dfrac{a+\Delta}{2},\,x_j-\dfrac{a-\Delta}{2}\right)\\[2ex]\dfrac{\Delta}{a}, & x\in\left(x_j-\dfrac{a-\Delta}{2},\,x_j+\dfrac{a-\Delta}{2}\right)\\[2ex]\dfrac{\Delta ax-x}{a}, & x\in\left(x_j+\dfrac{a-\Delta}{2},\,x_j+\dfrac{a+\Delta}{2}\right)\end{cases}\qquad(35)$$

and it is zero otherwise, where $\Delta ax=(a+\Delta)/2$. As a result, this weighting is identical to a mass assignment by linear interpolation. With these results it should now be clear that the mass density at a given grid point is

$$\rho(x_j)=\sum_{i\in\Delta_j}w(x_i-x_j),\qquad(36)$$

where the sum includes all the particles i whose area or volume overlap the grid cell Δ_j.

Putting all of these results together one obtains the following results for the weight of a particle to its neighboring grid cells:

$$w_{j+1}=\left(\frac{a-\Delta}{2}+x\right)\frac{1}{a}\qquad(37)$$

$$w_j=\min\left\{\left(\frac{a+\Delta}{2}-x\right)\frac{1}{a},\frac{\Delta}{a}\right\}\qquad(38)$$

$$w_{j-1}=\max\left\{\left(\frac{a-\Delta}{2}-x\right)\frac{1}{a},0\right\}.\qquad(39)$$

[7] Please note that as one sums Δv_i over all the particles of the same cell one obtains zero; i.e., there are no net forces from the drag term in a given cell.

All of the particles which overlap a cell contribute to the density and velocity at its grid point by this weighting scheme.

Likewise the force F_i on a particle i is the weighted sum of the forces from all the grid points which contain any fraction of that particle; that is,

$$F(x_i) = \sum_j F(x_j)\, w(x_i - x_j), \tag{40}$$

where the sum over x_j's is over all the grid points for which $|x_i - x_j| \in (a + \Delta)/2$ for each spatial dimension. Equations (36) and (40) will become useful in a later section as we study finite size particle effects.

2.4. *Momentum and Magnetic Flux Conservation*

Recall that the combined half time step pushers for the velocity give the velocity push for a full time step according to items 2 and 6 in Table I (we write things here in terms of the pressure tensor $\mathbf{\Pi}$ rather than density):

$$\mathbf{v}^{l+1/2} = \mathbf{v}^{l-1/2} + \left\{ \frac{n_0}{n_g^l} \left[-\nabla \cdot \left(\frac{B^2}{2} \bar{\bar{1}} - \mathbf{BB} \right) \right]^l - \nabla \cdot \mathbf{\Pi}^l + f(\mathbf{v}_f^l - \mathbf{v}_i^l) \right\} \Delta t. \tag{41}$$

Summing over all particles in the system gives

$$\sum_{\forall i} (\mathbf{v}_i^{l+1/2} - \mathbf{v}_i^{l-1/2}) = \sum_g \sum_{i \in g} \left\{ \nabla \cdot \left\{ \frac{n_0}{n_g} \left(\mathbf{BB} - \frac{B^2}{2} \bar{\bar{1}} \right) - \mathbf{\Pi} \right\}^l + f(\mathbf{v}_f^l - \mathbf{v}_i^l) \right\} \Delta t. \tag{42}$$

Here g simply stands for the grid cell and $\mathbf{\Pi}$ stands for the ion pressure tensor.

Since finite differences were used in computing all the derivatives (i.e., in computing the divergence of the kinetic pressure as well as the Maxwell stress tensor), then if one sums over all the grid points in the system, each such quantity will appear twice with opposite signs corresponding to the cell boundaries that are being shared between the neighboring cells, and they will thus add up to zero. There can, however, be contributions from the walls of the computation box, but for the periodic boundary conditions chosen here, their contributions give zero. For other cases momentum can be added to or removed from the system at the boundaries as the physics requires. Thus here Eq. (42) becomes

$$\sum_{\forall i} (\mathbf{v}_i^{l+1/2} - \mathbf{v}_i^{l-1/2}) = f \sum_g \sum_{i \in g} (\mathbf{v}_f^l - \mathbf{v}_i^l)\, \Delta t. \tag{43}$$

But $\sum_g \sum_{i \in g} \mathbf{v}_f^l = \sum_g n_g \mathbf{v}_f^l$ since $\mathbf{v}_f$ is a grid quantity. Also $\sum_g \sum_{i \in g} \mathbf{v}_i^l = \sum_g n_g \mathbf{v}_f^l$ by the definition of $\mathbf{v}_f$. This then proves that in such a system momentum is exactly conserved since the right-hand side of Eq. (43) is zero and, therefore,

$$\sum_{\forall i} (\mathbf{v}_i^{l+1/2} - \mathbf{v}_i^{l-1/2}) = 0. \tag{44}$$

Likewise, the magnetic induction equation can be used to yield the total magnetic flux in the system by summing the flux through cell areas over the whole system. We proceed as follows (the area of each cell, Δ_g^2, is unity due the normalization), using item 9 of Table I ($\hat{n}$ is normal to the grid cell with area Δ_g^2):

$$\sum_{\forall g} \hat{n} \cdot \left\{ \mathbf{B}^{l+1} \Delta_g^2 = \sum_{\forall g} \Delta_g^2 \mathbf{B}^l + \sum_{\forall g} \Delta_g^2\, \Delta t\, \nabla \times \left[\mathbf{v}_f^{l+1/2} \times \mathbf{B}^{l+1/2} + \lambda \frac{n_0}{n^{l+1/2}} \nabla \cdot \left(\frac{B^2}{2} \bar{\bar{1}} - \mathbf{BB} \right)^{l+1/2} \right] \right\}, \tag{45}$$

which gives

$$\sum_{\forall g} (\Phi_g^{l+1} - \Phi_g^l) = \sum_{\forall g} \Delta_g^2 (\mathbf{B}^{l+1} - \mathbf{B}^l) \cdot \hat{n} = \sum_{\forall g} \Delta_g^2\, \Delta t \left\{ \nabla \times \left[\mathbf{v}_f^{l+1/2} \times \mathbf{B}^{l+1/2} + \lambda \frac{n_0}{n^{l+1/2}} \nabla \cdot \left(\frac{B^2}{2} \bar{\bar{1}} - \mathbf{BB} \right)^{l+1/2} \right] \right\} \cdot \hat{n}, \tag{46}$$

where Φ is simply the magnetic flux.

All the quantities on the right-hand side are derivatives and so, upon summation, will give zero as in the case of the momentum and this proves our assertion, i.e.,

$$\Phi^{l+1} = \Phi^l. \tag{47}$$

2.5. *Numerical Stability Analysis*

In order to obtain the Courant–Fredricks–Lewy (CFL) condition for the model, the difference equations for the model (obtained from the differential equations for the problem by discretizing them) must be considered. We follow the method of Potter [7]; i.e., obtain the integration-time pusher operator from the difference equations assuming a spatially uniform system and solve them in Fourier space and obtain non-local results. We shall do the stability analysis once with and once without the Hall term to see the effects of the Hall term on such an analysis. Thus

for comparison purposes, identical physical conditions must be considered.

Recall that the differential Equations (12) and (13) formed the basis of the model. In this analysis, we consider parallel propagating Alfven waves only (i.e., whistler and ion cyclotron waves), since in the perpendicular direction the magnetoacoustic waves are unaffected by the addition of the Hall term. We also consider low β plasmas, in which case the pressure effects which give rise to the sound velocity can be neglected since the Alfven velocity is much greater than the sound velocity; and since the highest velocities are most restrictive for stability, the sound waves can be neglected. Equation (12), after neglecting the pressure term and upon linearization, gives ($\mathbf{B}_0 = B_0\hat{x}$):

$$\rho \frac{dv_y}{dt} = \frac{B_0}{4\pi}\frac{\partial B_y}{\partial x}, \quad \rho \frac{dv_z}{dt} = \frac{B_0}{4\pi}\frac{\partial B_z}{\partial x}. \tag{48}$$

Using Eq. (13), the differential equations for the two non-zero field components (B_y and B_z) in their pseudo-conservative forms are

$$\frac{\partial B_y}{\partial t} - B_0\frac{\partial v_y}{\partial x} - \bar{\alpha}B_0\frac{\partial^2 B_z}{\partial x^2} = 0 \tag{49}$$

$$\frac{\partial B_z}{\partial t} - B_0\frac{\partial v_z}{\partial x} + \bar{\alpha}B_0\frac{\partial^2 B_y}{\partial x^2} = 0. \tag{50}$$

Before obtaining the difference versions of Eqs. (49) and (50) we shall use them to gain an important insight into the diffusive nature of the Hall term and its consequences. To do so, let us multiply Eq. (49) by i and add it to Eq. (50), keeping only the time derivative and the Hall term. With $\mathscr{B} = B_z + iB_y$, that operation will result in the equation

$$\frac{\partial \mathscr{B}}{\partial t} - i\bar{\alpha}B_0\frac{\partial^2 \mathscr{B}}{\partial x^2} = 0. \tag{51}$$

This is a diffusion equation with an imaginary diffusion coefficient. Assuming $\mathscr{B} \propto e^{i(kx-\omega t)}$, the dispersion relation for Eq. (51) will be

$$\omega = k^2\bar{\alpha}B_0. \tag{52}$$

The solutions to Eq. (51) are thus oscillatory and not damped as in the usual diffusion equation. Furthermore, the phase velocity of the resulting waves are

$$v_p = \frac{\omega}{k} = k\bar{\alpha}B_0. \tag{53}$$

This simply means that at higher k values the phase velocity v_p becomes larger; i.e., the Hall term gives rise to high phase velocity waves and these will thus concern us most with regards to stability. For this reason, later on, when we attempt to obtain the stability condition for the case with the Hall term present, the Hall term becomes the most important term in the analysis.

Next using Eqs. (48)–(50), after combining the auxiliary and the main steps of the Lax–Wendroff scheme and assuming $\mathbf{B}$ and $\mathbf{v}$ to have the form (l refers to the time step and i inside the parenthesis to the grid location along x)

$$(\mathbf{B}^l, \mathbf{v}^l) = (\hat{\mathbf{B}}^l, \hat{\mathbf{v}}^l)\, e^{i(k_x i\,\Delta x - l\omega\,\Delta t)}, \tag{54}$$

we obtain the following integration operators for $\mathbf{B}_y$ and $\mathbf{B}_z$ ($\sigma = k_x\,\Delta x$):

$$B_y^{l+1} = \left\{1 - \frac{ic_A^2(\Delta t)^2\sin^2\sigma}{2(\Delta x)^2\sin(\omega\,\Delta t/2)} \times\left[\cos^2\frac{\sigma}{2} - \frac{ic_A^2(\Delta t)^2\sin^2\sigma}{4(\Delta x)^2\sin(\omega\,\Delta t/2)}\right] - \frac{\bar{\alpha}^2B_0^2\sin^4\sigma}{(\Delta x)^4}\frac{(\Delta t)^2}{2}\right\}B_y^l + \left\{\frac{ic_A^2(\Delta t)^3\sin^4\sigma}{2(\Delta x)^4\sin(\omega\,\Delta t/2)} - \frac{\sin^2\sigma\cos^2(\sigma/2)}{(\Delta x)^2}\Delta t\right\}\bar{\alpha}B_0B_z^l \tag{55}$$

and

$$B_z^{l+1} = \left\{1 - \frac{ic_A^2(\Delta t)^2\sin^2\sigma}{2(\Delta x)^2\sin(\omega\,\Delta t/2)} \times\left[\cos^2\frac{\sigma}{2} - \frac{ic_A^2(\Delta t)^2\sin^2\sigma}{4(\Delta x)^2\sin(\omega\,\Delta t/2)}\right] - \frac{\bar{\alpha}^2B_0^2\sin^4\sigma}{(\Delta x)^4}\frac{(\Delta t)^2}{2}\right\}B_z^l - \left\{\frac{ic_A^2(\Delta t)^3\sin^4\sigma}{2(\Delta x)^4\sin(\omega\,\Delta t/2)} - \frac{\sin^2\sigma\cos^2(\sigma/2)}{(\Delta x)^2}\Delta t\right\}\bar{\alpha}B_0B_y^l. \tag{56}$$

Since $B_z^{l+1} = e^{-i\omega\,\Delta t}B_z^l$ and $B_y^{l+1} = e^{-i\omega\,\Delta t}B_y^l$, then taking $g = e^{-i\omega\,\Delta t}$, the Von Neumann stability condition ($|B^{l+1}/B^l| \leqslant 1$) reduces to $|g| \leqslant 1$. Thus, one needs to use Eqs. (55) and (56) to obtain g, from which one can determine the stability condition. The two equations (55) and (56) reduce upon that substitution to

$$(g - x_1)\,B_y^l + y_1B_z^l = 0 \tag{57}$$

$$-y_1B_y^l + (g - x_1)\,B_z^l = 0, \tag{58}$$

where x_1 and y_1 are simply

$$x_1 = 1 - \frac{ic_A^2(\Delta t)^2 \sin^2\sigma}{2(\Delta x)^2 \sin(\omega\,\Delta t/2)}\left[\cos^2\frac{\sigma}{2} - \frac{ic_A^2(\Delta t)^2 \sin^2\sigma}{4(\Delta x)^2 \sin(\omega\,\Delta t/2)}\right] - \frac{\bar{\alpha}^2 B_0^2 \sin^4\sigma}{(\Delta x)^4}\frac{(\Delta t)^2}{2} \tag{59}$$

$$y_1 = \left\{\frac{ic_A^2(\Delta t)^3 \sin^4\sigma}{2(\Delta x)^4 \sin(\omega\,\Delta t/2)} - \frac{\sin^2\sigma\cos^2(\sigma/2)}{(\Delta x)^2}\Delta t\right\}\bar{\alpha}B_0. \tag{60}$$

we next make the substitution $\Delta x = \Delta y = \Delta$. The value of g is then determined by setting the determinant of the coefficients of B_y^l and B_z^l in Eqs. (57) and (58) equal to zero; i.e.,

$$\begin{vmatrix} g - x_1 & y_1 \\ -y_1 & g - x_1 \end{vmatrix} = 0. \tag{61}$$

Equation (61) reduces to

$$(g - x_1)^2 + y_1^2 = 0 \tag{62}$$

and therefore the solutions for g are simply $g = x_1 \pm iy_1$, which upon substitution of x_1 and y_1 give rise to

$$g_\pm = 1 - \frac{(\Delta t)^4 c_A^4 \sin^4\sigma}{8(\Delta)^4 \sin^2(\omega\,\Delta t/2)} - \bar{\alpha}^2 B_0^2 \frac{\sin^4\sigma}{2\Delta^4}(\Delta t)^2 \mp \frac{\bar{\alpha}B_0 c_A^2(\Delta t)^3 \sin^4\sigma}{2\Delta^4 \sin(\omega\,\Delta t/2)} + i\left[-\frac{c_A^2(\Delta t)^2 \sin^2\sigma\cos^2(\sigma/2)}{2\Delta^2 \sin(\omega\,\Delta t/2)} \mp \frac{\bar{\alpha}B_0\,\Delta t \sin^2\sigma\cos^2(\sigma/2)}{\Delta^2}\right]. \tag{63}$$

When no Hall term is present (i.e., $\bar{\alpha} = 0$), this reduces to

$$g = 1 - \frac{(\Delta t)^4 c_A^4 \sin^4\sigma}{8\Delta^4 \sin^2(\omega\,\Delta t/2)} - i\frac{c_A^2(\Delta t)^2 \sin^2\sigma\cos^2(\sigma/2)}{2\Delta^2 \sin(\omega\,\Delta t/2)}. \tag{64}$$

From $g = e^{-i\omega\,\Delta t} \simeq 1 - i\omega\,\Delta t$, with $\omega = \omega_R + i\omega_I$, the following dispersion relation is obtained:

$$\omega_R = \frac{c_A \sin\sigma\cos(\sigma/2)}{\Delta}. \tag{65}$$

Using this in Eq. (64) gives

$$g = 1 - \frac{(\Delta t)^2 c_A^2 \sin^2\sigma}{2\Delta^2\cos^2(\sigma/2)} - \frac{i\,\Delta t}{\Delta}c_A \sin\sigma\cos(\sigma/2). \tag{66}$$

The Von Neumann stability condition ($|g| \leqslant 1$) will then result in the following stability criterion:

$$\Delta t \leqslant \sqrt{2}\frac{\Delta}{c_A}. \tag{67}$$

Here c_A is to be understood as being the highest speed of propagation that can exist in the system. This result shows an improvement in the allowed time step compared with the $\Delta t \leqslant (\sqrt{3}/2)(\Delta/c)$ obtained by Tajima *et al.* [2].[8]

Next, in order to obtain the stability condition for the case with the Hall term present, we keep only the time difference term and the Hall term. As we saw above, the Hall term gives a diffusion equation (with an imaginary diffusion coefficient) and these give high phase velocity disturbances for large k; this term thus dominates the stability considerations. We can then compare the resulting condition with that obtained by Tajima *et al.* [2] as those authors carried out a similar analysis.

Keeping only the time difference and the Hall terms in Eqs. (49) and (50) gives

$$g_\pm = 1 - \bar{\alpha}^2 B_0^2 \frac{\sin^4\sigma}{2\Delta^4}(\Delta t)^2 \mp i\frac{\bar{\alpha}B_0\,\Delta t \sin^2\sigma\cos^2(\sigma/2)}{\Delta^2}. \tag{68}$$

Using the Von Neumann condition $|g| \leqslant 1$, we obtain the following stability condition[9]:

$$\Delta t \leqslant 1.66\frac{\Delta^2}{\bar{\alpha}B_0} = 1.66\frac{\Delta^2}{c_A^2/\omega_{ci}}; \tag{69}$$

please note that here we used $\bar{\alpha}B_0 = c_A^2/\omega_{ci}$, as defined in Eq. (27).

This result is physically reasonable in light of the fact that the Hall term acts like a diffusion term (with an imaginary coefficient), and the right-hand side of Eq. (69) is just the diffusion time across a scale length Δ times a constant 1.66. This result also demonstrates an improvement to that obtained by Tajima *et al.* [2] and the superiority of the Lax–Wendroff technique used in this model over the simpler Lax technique employed there.

The above analysis equally applies to the three-dimensional case, since parallel propagating waves were considered in the analysis. In the simulations which were performed here, $c_A = 4c_s$ and $\omega_{ci} = 4c_s/\Delta$. As a result

[8] c is the highest allowable speed of propagation in the system; i.e., c_A here.

[9] Brunel *et al.* [3] did use the Lax–Wendroff technique after Tajima *et al.* [2]. They obtained a stability condition ($\Delta t \leqslant \sqrt{2}\,\Delta/c$; c is the highest speed of propagation) for the case without the Hall term present. They did not have the Hall term present and thus did not obtain a condition for that case. As a result we mainly use Tajima's result for making comparisons.

$\Delta t \leqslant \sqrt{2}\,(\Delta^2/c_A^2/\omega_{ci}) = 0.35$ for the more restrictive case at which the Hall term is not present. In the simulation runs presented in this paper, however, a $\Delta t = 0.2$ was used and the code in both the two- and three-dimensional runs was stable, with $v_t = 0.1 c_s$ as the initial random thermal jitters of the ion fluid particles.

2.6. *Finite Grid Size Effects*

Tajima *et al.* [2] has done a similar analysis using the one-step Lax method for the model with the Hall term, while Brunel *et al.* [3] has done so using the two-step Lax–Wendroff scheme, but for the case in which the Hall term is not present. Here we do the analysis for the case when the Hall term is present in the model which uses the two-step Lax–Wendroff scheme for pushing the magnetic field.

At this point, we need to obtain the dispersion relation for the difference scheme. However, for comparison purposes, we shall need the corresponding dispersion relation of the differential equation. Recall that for propagation of the waves parallel to $\mathbf{B}_0$ which is along $x(k_{\|} = k = k_x)$, for $c_s = 0$, the analytic dispersion relation becomes

$$\omega = k_x c_A \sqrt{1 + \frac{k_x^2 c_A^2}{4\omega_{ci}^2}} \pm \frac{k_x^2 c_A^2}{2\omega_{ci}} \tag{70}$$

as given by Eq. (29). For small wave numbers this reduces to

$$\omega \cong k_x c_A \pm \frac{k_x^2 c_A^2}{2\omega_{ci}} + O(k_x^3). \tag{71}$$

Substituting $g_{\pm} = e^{-i\omega\,\Delta t} \cong 1 - i\omega\,\Delta t$ in Eq. (63) we obtain the following dispersion relation for the difference equations for this case $(\omega = \omega_R + i\omega_I)$:

$$\omega_R = \frac{c_A}{\Delta} \sin\sigma \cos\frac{\sigma}{2} \pm \frac{\bar{\alpha} B_0}{2\Delta^2} \sin^2\sigma \cos^2\frac{\sigma}{2} + O(\sin^3\sigma) \tag{72}$$

$$\omega_I = -\frac{\Delta t\, c_A^2 \sin^2\sigma}{2\Delta^2 \cos^2(\sigma/2)} + O(\sin^3\sigma). \tag{73}$$

For small wave numbers then, Eqs. (72) and (73) will reduce $(\bar{\alpha} B_0 = c_A^2/\omega_{ci})$

$$\omega_R = c_A k_x \mp \frac{k_x^2 c_A^2}{2\omega_{ci}} + O(k_x^3 \Delta^3) \tag{74}$$

$$\omega_I = -\frac{\Delta t\, c_A^2 k_x^2}{2} + O(k_x^3 \Delta^3). \tag{75}$$

Clearly then for small wave numbers k_x, Eq. (72) agrees with Eq. (71). The first term gives rise to the Alfven dispersion relation $\omega = k_x c_A$. The second term originates from the presence of the Hall term and simply splits the Alfven branch into the whistler (with the plus sign) and the ion cyclotron (with the minus sign) branches, respectively. The imaginary part of ω, ω_I, as we see from Eqs. (73) and (75), is proportional to Δt; i.e., it should arise from finite differencing in time. It merely acts as a damping term.

Finite grid effects come into play in higher powers of $k_x \Delta$ as $\sin k_x \Delta$ and $\cos k_x \Delta$ are expanded. In regards to the first term, as k_x increases the dispersion relation deviates from $\omega = k_x c_A$ and bends down $(\omega < k_x c_A)$. The effect on the second term (the Hall term) is to lower the frequency of the whistler branch and raise that of the ion-cyclotron branch; i.e., this makes the split between them smaller.

The imaginary part of ω (ω_I in Eqs. (73) and (75)), simply acts as a damping term and arises due to the finite differencing as already explained. As we see, it is of the order of k_x^2 and higher. It therefore effects high wave number modes most. This can be understood since it is these modes which are most affected by finite differencing. Often the act of finite differencing causes the generation of unphysical behavior of the high mode numbers which can drastically affect the reliability of the model if these modes are important. In particular we observed such waves upon applications of the model to some phenomenon in which high thermal velocities for the particles had to be used; we eliminated large k mode effects by a process of smoothing. That work will appear in a separate publication of this journal.

In conclusion, upon comparison of Eqs. (71) and (72), for k_x small enough to be away from $k_x = \pi/2\Delta$, k_x can be very well approximated by $k_x \to k_x(\sin(k_x\Delta)/k_x\Delta)$, and the dispersion relation for the finite difference model (Eq. (72)) agrees quite well with that for the differential equation. This criterion can be generalized to other arbitrary wave numbers (k_x, k_y, k_z). The relation between the differential and difference dispersion relationships will be quite similar to what was found here. This is very well illustrated in the "tests of the model" section.

2.7. *Finite Particle Size Effects*

In obtaining spatial derivatives in this model, use has only been made of a finite differencing technique. For the procedure described, the finite size of the particles and their shape arise only through their weighted contributions to each grid point as can be seen through Eq. (40).

It is often useful to introduce particles of a finite size and a suitable smooth shape which is independent of the grid size; this allows us to introduce an independent fine scale smoothing and to study its effects on the results. This is most easily accomplished in Fourier transform space as demonstrated by Birdsall *et al.* [6]. In order to obtain a rough estimate of finite size particle effects that go with this, we go back to Eqs. (12) and (13). For purposes of under-

standing we treat the simplest case and just look at the analytic dispersion relation for Alfven waves (i.e., we eliminate the pressure and the Hall terms for simplicity); we then need only consider the $\mathbf{j}\times\mathbf{B}/c$ force in the equation of motion.

To obtain the force on particle i we must average the $\mathbf{j}\times\mathbf{B}/c$ force over the grid cells j that the particle i overlaps using area weighting just as in Eq. (40). Likewise to obtain the fluid velocity at grid cell j one must compute the weighted sum of the velocities of all the particles which overlap that grid cell. One then immediately obtains the following set from Eqs. (12) and (13):

$$\rho\frac{d\mathbf{v}(\mathbf{r}_i)}{dt}=-\frac{1}{4\pi}\sum_j w(\mathbf{r}_i-\mathbf{r}_j)(\mathbf{B}\times(\nabla\times\mathbf{B}))\ [\text{at } \mathbf{r}_j] \tag{76}$$

$$\frac{\partial\mathbf{B}(\mathbf{r}_j)}{\partial t}=(\nabla\times(\mathbf{v}\times\mathbf{B}))\ [\text{at } \mathbf{r}_j]$$

$$=\nabla\times\left(\sum_{i\in\Delta_j} w(\mathbf{r}_j-\mathbf{r}_i)\,\mathbf{v}(\mathbf{r}_i)\times\mathbf{B}(\mathbf{r}_j)\right) \tag{77}$$

(the index i refers to the particle positions, while the j index refers to the grid positions).

In a system with a very large number of grid points and particles, the variables $\mathbf{r}_j$ and $\mathbf{r}_i$ can be thought of as changing continuously and therefore the summations over j and i in Eqs. (76) and (77) can be approximated by integrations. The right-hand sides of Eqs. (76) and (77) will appear as convolutions in which case the variables of integration will be the grid and particle positions, respectively; e.g., Eqs. (76) and (77) can be approximated by the following pair:

$$\rho\frac{d\mathbf{v}}{dt}(\mathbf{r})=-\frac{1}{4\pi}\int_{-\infty}^{+\infty} w(\mathbf{r}-\xi)(\mathbf{B}\times(\nabla\times\mathbf{B}))\ [\text{at } \xi]\,d\xi \tag{78}$$

$$\frac{\partial\mathbf{B}}{\partial t}(\mathbf{r})=\int_{-\infty}^{+\infty}\nabla\times(w(\mathbf{r}-\zeta)\,\mathbf{v}(\zeta)\times\mathbf{B}(\mathbf{r}))\,d\zeta. \tag{79}$$

Please note that the weight for grid cells which do not overlap particle i are zero and vice versa. This, therefore, justifies the $-\infty$ to $+\infty$ limit on the integrations.

In this case, upon linearization and Fourier transforming of Eqs. (78) and (79), these equations reduce to

$$\omega\mathbf{v}(\mathbf{k})=\frac{1}{4\pi\rho_0}w(\mathbf{k})\,\mathbf{B}_0\times(\mathbf{k}\times\mathbf{B}(\mathbf{k}))$$

$$=\frac{w(\mathbf{k})}{4\pi\rho_0}\{\mathbf{k}(\mathbf{B}_0\cdot\mathbf{B}(\mathbf{k}))-\mathbf{B}(\mathbf{k})(\mathbf{B}_0\cdot\mathbf{k})\} \tag{80}$$

$$-\omega\mathbf{B}(\mathbf{k})=\mathbf{k}\times(w(\mathbf{k})\,\mathbf{v}(\mathbf{k})\times\mathbf{B}_0)$$

$$=w(\mathbf{k})[\mathbf{v}(\mathbf{k}\cdot\mathbf{B}_0)-\mathbf{B}_0(\mathbf{k}\cdot\mathbf{v})]. \tag{81}$$

For parallel propagating Alfven waves $\mathbf{k}\cdot\mathbf{v}=\mathbf{B}_0\cdot\mathbf{B}(\mathbf{k})=0$. Then substituting Eq. (80) in Eq. (81) gives the dispersion relation

$$\omega^2=w^2(\mathbf{k})\,k^2c_A^2. \tag{82}$$

This is then how the weight factor affects the analytic dispersion relation of Alfven waves.

Now given $w(x)$ in Eq. (35), $w(\mathbf{k})$ is simply

$$w(k)=\frac{1}{\Delta ax}\int_{-\Delta ax}^{+\Delta ax} w(x)\,e^{-ikx}\,dx \tag{83}$$

(please recall that $\Delta ax=(\Delta+a)/2$, where a is just the particle size), which after a straightforward calculation using the weighting defined earlier, gives the result

$$w(k)=\frac{\sin(k\Delta/2)\sin(ka/2)}{(k^2a\,\Delta ax/4)}. \tag{84}$$

Recall that the finite grid effects also result in $k\to k(\sin k\Delta/k\Delta)$. The combined finite grid and particle size effects results in modifying the dispersion relation for Alfven waves as

$$\omega^2=\frac{\sin^2(k\Delta/2)\sin^2(ka/2)}{(k^2a\,\Delta ax/4)^2}\frac{\sin^2 k\Delta}{(k\Delta)^2}k^2c_A^2. \tag{85}$$

Consequently, the combined effect is like replacing k by

$$\frac{\sin(k\Delta/2)\sin(ka/2)}{a\,\Delta axk^2/4}\frac{\sin k\Delta}{k\Delta}k$$

in the analytic dispersion relation. This effect will be shown briefly in the next section.

3. TESTING THE CODE

As mentioned, we have constructed both two- and three-dimensional versions of the code and we have tested them by looking at small amplitude (linearized) wave propagation in a uniform plasma. First we tested the two-dimensional version; its geometry is shown in Fig. 3. For this model $\mathbf{k}$ was restricted to the x, y plane but the velocity and $\mathbf{B}$ were allowed to also have z components.

The first case we tested was the case of $\mathbf{B}_0$ parallel to $\hat{x}$ and $\mathbf{k}=k_{\|}=k$ was simply along the $\hat{x}$ direction. We tested the code with and without the Hall term; i.e., we ran cases in which the coefficient of the Hall term, λ (defined by the items 5 and 9 in Table I), was set equal to zero and one. The differences were then observed. The frequencies of the waves were determined using the correlation technique discussed in Dawson [8]. The results of these measurements are summarized in Fig. 4. The two branches with ·'s are obtained

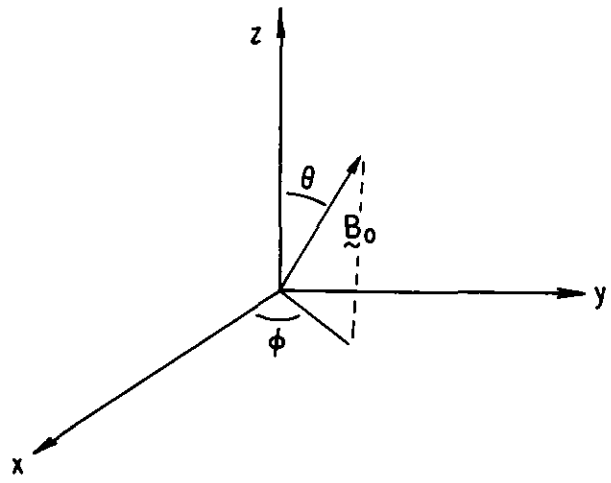

FIG. 3. Geometry of the model.

from the Hall term version of the code; the x's are from the pure MHD version of the code. We see that the Hall term causes the Alfven wave modes with frequencies at $\pm\omega_A$ to split into the ion cyclotron and the whistler wave modes. The turning down of the whistler wave at high k (wave numbers) is due to the finite grid as well as finite particle size effects discussed in previous sections. This result agrees with that obtained by Tajima *et al.* [2], who used the one-step Lax method in pushing the **B**, as opposed to the two-step Lax–Wendroff method employed here; our technique, however, allowed for larger time steps, as already mentioned.

The next case we studied was for $\mathbf{B}_0$ parallel to $\hat{z}$; thus $\mathbf{k}$ was perpendicular to $\mathbf{B}_0$—these were the magnetoacoustic cases. The Hall term does not split this branch; however, one does see a zero frequency branch appearing which arises simply from pressure striations confined by the magnetic field. In Fig. 5 we include not only the pure differential dispersion relation obtained by finding the roots of Eq. (103) with $\theta = 0°$, $\mathbf{k} = k_x$, but also the roots of that equation with the wave vector k replaced by $k(\sin(k\Delta)/k\Delta)$ to observe the finite grid effects, and the roots with k being replaced by

$$k \frac{\sin k\Delta}{k\Delta} \frac{\sin(k\Delta/2)\sin(ka/2)}{a\,\Delta a x k^2/4}$$

to observe the combined effects of finite grid and particle size effects. All these results are shown in the same plot along with the simulation results in order to demonstrate the agreement with the results obtained with regards to these effects in the previous sections.

As a severe test of the model we ran a case of almost perpendicular propagation. The reason for this being that, as mentioned in the analytic treatment section, waves almost

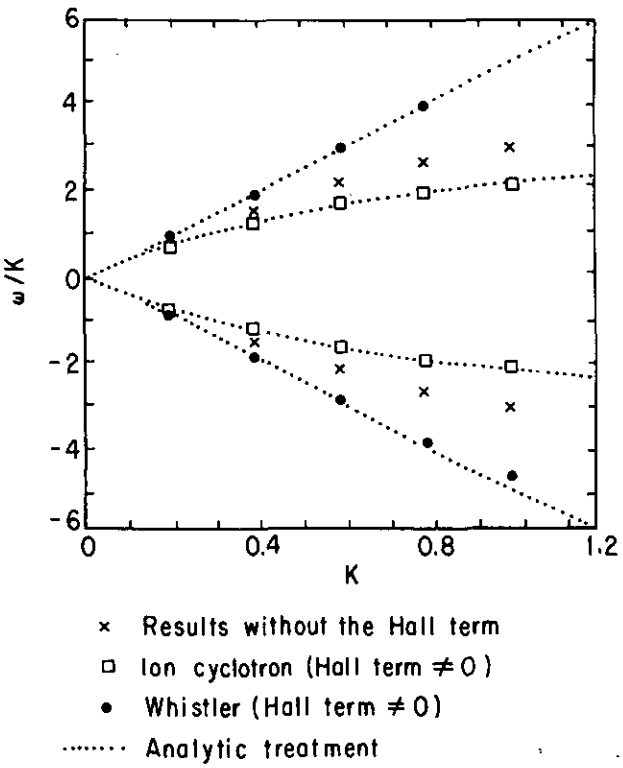

FIG. 4. Dispersion relation for the model with and without the Hall term (propagation parallel to $\mathbf{B}_0$).

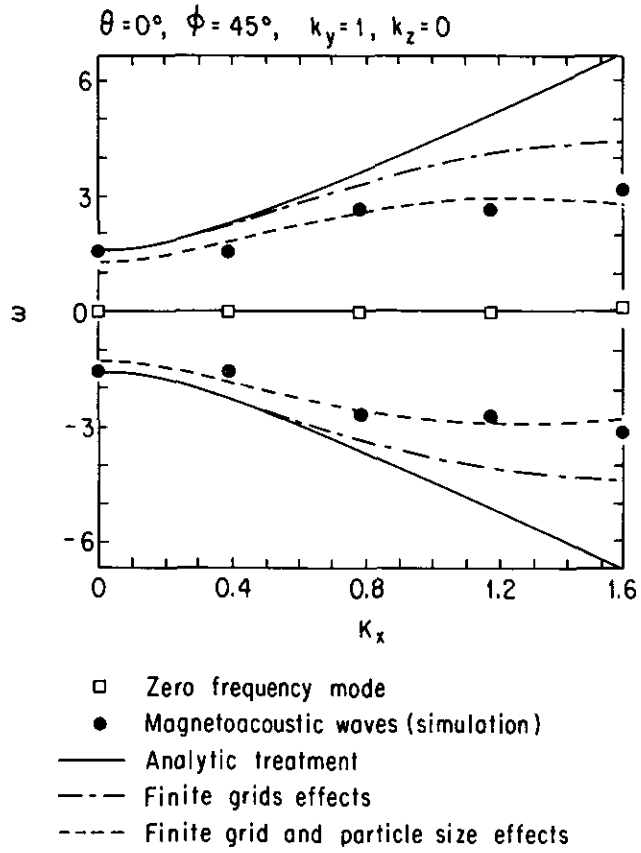

FIG. 5. Dispersion relation for the waves propagating perpendicular to $\mathbf{B}_0$.

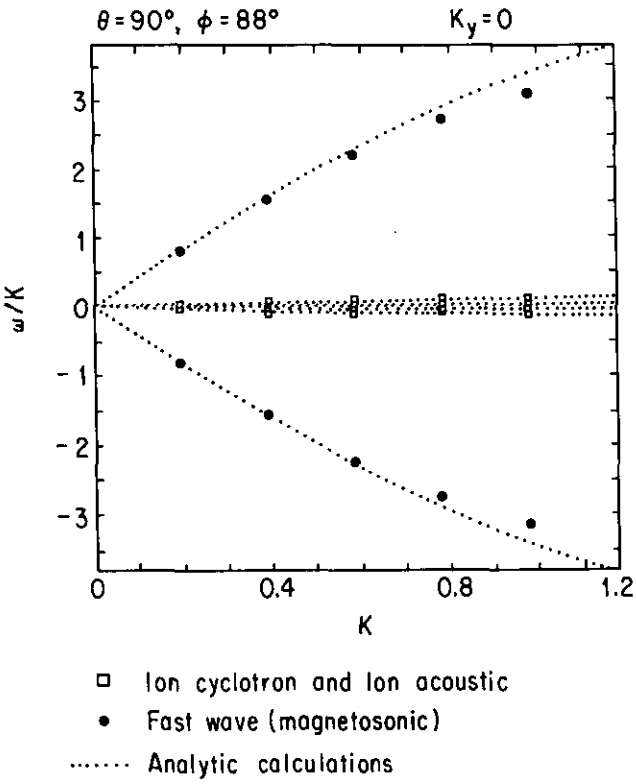

FIG. 6. Dispersion relation for the almost perpendicular propagation.

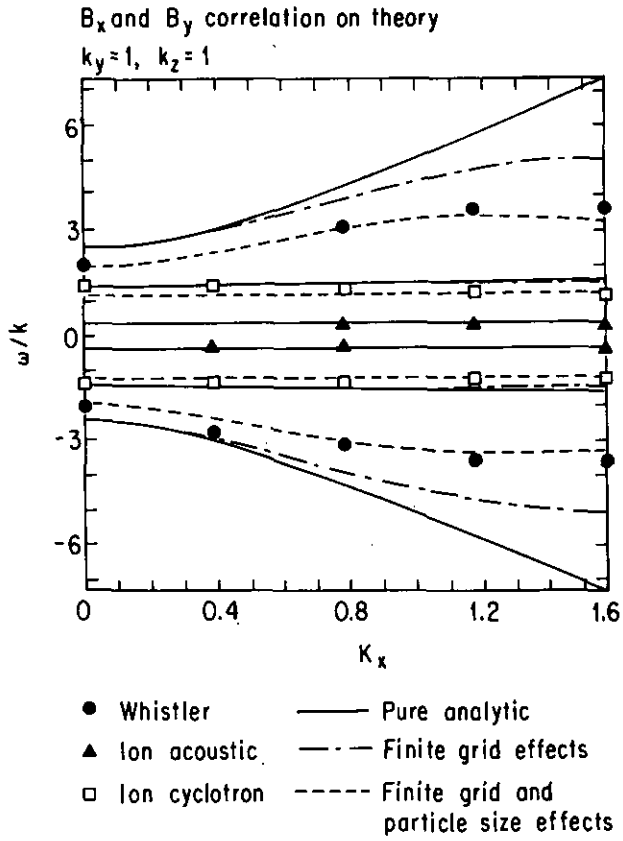

FIG. 7. Dispersion relation from the three-dimensional model, fixed $k_y = k_z = 1$.

perpendicular to $\mathbf{B}_0$ produce large currents parallel to $\mathbf{B}_0$ and thus strain the numerical procedures. If the code is correct it should give the analytically predicted frequencies. For this reason the results of the extreme case in which $\theta = 90°$, $\varphi = 88°$, and $\mathbf{k} = k_x$ (i.e., $\mathbf{B}_0$ almost parallel to $\hat{y}$ and $\mathbf{k}$ in the $\hat{x}$ direction) are shown in Fig. 6. The analytic prediction along with the simulation results are shown in that figure. The ion cyclotron branch, the ion acoustic branch, and the Alfven (or whistler) branches are shown and they agree very well with the theory.

Finally, we have constructed a fully three-dimensional model including the Hall term. It is the same as the 2D model except that $\mathbf{k}$ can now have any direction. Figure 7 shows dispersion results (ω versus k_x) for $k_y = k_z = 1$. These modes are quite oblique and also the code is now a three-dimensional one and will manifest most the finite grid as well as the finite size particle effects. For that reason, the results of the pure differential dispersion relation, as well as analytic forms including finite grid and particle size corrections, are shown on this plot along with simulation results. Clearly we see that, finite grid and finite particle size effects cause a substantial amount of dispersion at the higher wave numbers; this is particularly strong for the whistler branch which has the highest frequency. However, the results show fairly good agreement for a relatively coarse grid system of 32^3 grids in all directions. To see one application of the model, please refer to Section 4.

4. APPLICATION: WAVE ACTIVITY IN FRONT OF THE COMETS

The study of shock in fronts of comets and planets have emerged as a central area of research for space plasma physics; i.e., shocks contribute to the energy for much of the radiation and wave activity observed around the comets and planets. Studies of these waves therefore form an important subclass of shock studies. The particle MHD code, with its rich wave modeling capability thus serves as an invaluable tool for such studies.

We used our code to model the AMPTE (active magnetospheric particle tracer explorer) experiments (performed in July and December 1984) and published in extensive articles in *Nature* magazine [10–15].

In those experiments two satellites, IRM (ion release module) and UKS (United Kingdom subsatellite) recorded magnetic wave amplitudes as they travelled through the cloud and into the shock front region. They recorded wave activity at the shock front which was conjectured to be due to magnetoacoustic and ion acoustic waves generated in the shock region and propagating upstream into the solar wind.

We used the two-dimensional version of the code to model the experiment. The geometry is depicted in Fig. 8;

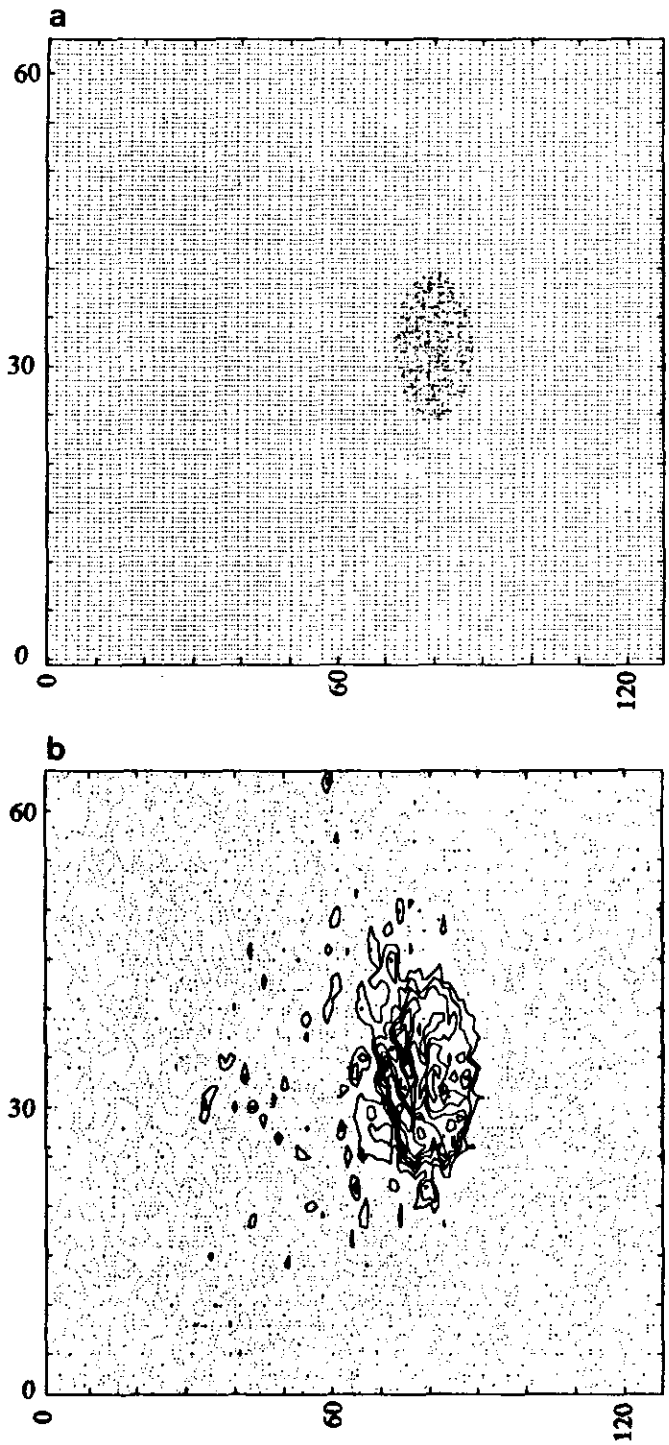

FIG. 8. (a) The initialization of the particles in configuration space. (b) Contour plot of the density after three gyroperiods.

i.e., the system size was 128×64 grid spacings and the comet was initially located at the grid point $(80-32)$ with its unionized gas flowing radially outward. The gas gradually ionized as the cloud expanded to model solar ionization. The $\mathbf{B}_0$ field was taken to be along the z axis. In the simulations we stored the magnetic field and densities at certain

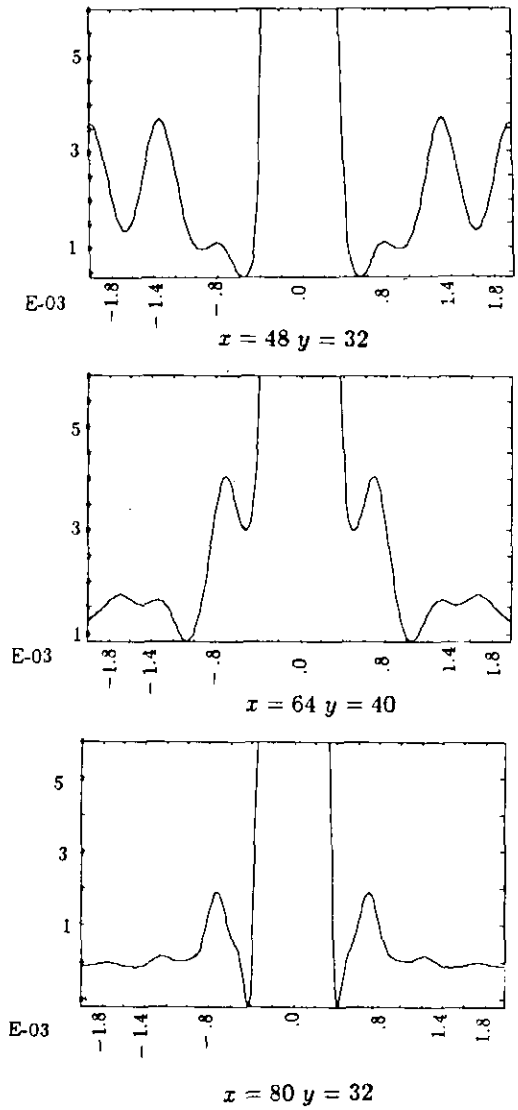

FIG. 9. The power spectra peaks at three locations in front of the shock using the model; the system size was 128×64 and the comet was centered at $(80-32)$.

locations (in the shock region) on the mesh as a function of time. We then took their Fourier transforms in time to investigate the wave activity. The method is essentially identical to the power spectra method described by Dawson [8], except that here we are dealing with a fairly inhomogeneous plasma and one that has motion. Therefore, the power spectra peaks are not epected to be as sharp as those of a homogeneous plasma, and their frequencies will be slightly doppler shifted.[10]

The simulations gave reasonable peaks at fairly well-defined frequencies. Figure 9 shows some of the power

[10] In the experiment, the UKS satellite had almost no relative motion with respect to the IRM satellite which made the release. In the simulations also the wave analysis is done in the plasma rest frame at all points. As a result, the frequency doppler shift does not play an important role in either case.

spectra of the simulations. The power spectra are those of the magnetic field. The numbers underneath each picture are just the coordinates of the point at which **B** was analyzed; i.e., they all correspond to points in the shock region for a comet located at (80 – 32). As we see the peaks consistently occur at $\omega \sim 0.8$ and $\omega \sim 1.2$. The original ω_{ci} was $\omega_{ci} = 0.2$ in this simulation.

To identify which waves these peaks correspond to we solved the analytic dispersion relation (Eq. (103)) with $\theta = 0$, $\phi = 0$, $c_A = 0.2$ and $c_s = 1$. We only looked at waves with $k_z = 0$. The results are depicted in Fig. 10. As mentioned earlier, the outermost curves correspond to the pure analytic solution, the middle ones to the analytic forms including the finite grid corrections, and the innermost plots to the analytic forms including finite grid as well as finite particle size corrections. The innermost plots best compare the simulation results of Fig. 9, while their corresponding pure analytic plots enables us to identify the nature of the waves.

The analytic curves of the Fig. 10 correspond to

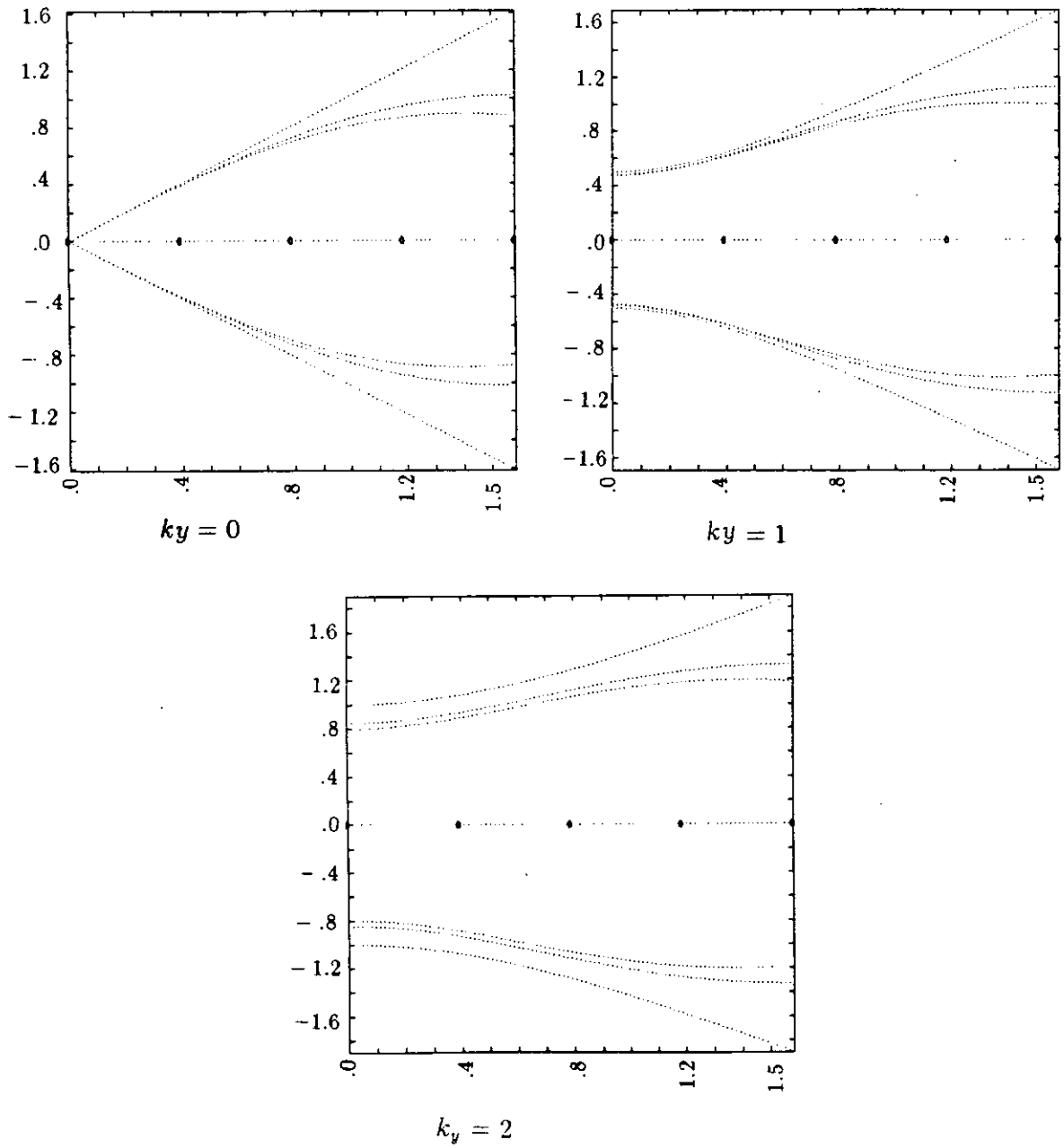

FIG. 10. Roots of the analytic dispersion relation (ω vs k_x for fixed k_y) for $\mathbf{B}_0$ along the z axis and $k_z = 0$. Outermost curve is pure analytic; the middle and innermost curves have finite grid and particle size corrections.

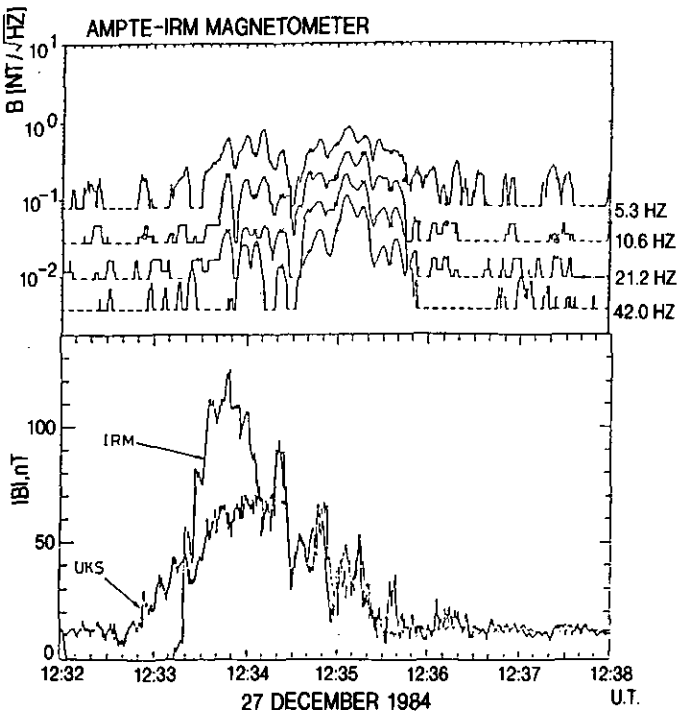

FIG. 11. Some of the experimental records of the wave activity as recorded by the IRM satellite [16].

magnetoacoustic waves since for them $k_z = 0$ and $\mathbf{B}_0$ is along the z axis. In the innermost curves as we see that, for small k_x, ω rises linearly and then becomes fairly dispersive and flattens to a roughly constant value between $\omega \sim 0.7$ to $\omega \sim 1.2$, depending on its k_y value as we see from the three pictures. Those are exactly the frequencies of the power spectra peaks depicted in Fig. 9.

Figure 11 [16] shows experimental results of the wave activity observed by the IRM satellite. The experimental ω_{ci} (the proton gyrofrequency) can be shown to be $\omega_{ci} = 0.96$ Hz, using the ambient magnetic field of 10 nanotesla in $e\mathbf{B}_0/M$ (e and M are the proton charge and mass, respectively). That simply means that the frequency of 5.3 Hz in the top plot of Fig. 11 is $5.53\omega_{ci}$. On the other hand, in the simuations of this subsection $\omega_{ci} = 0.2$. As a result the simulation peaks with frequencies 0.8 and 1.2 in Fig. 9 correspond to frequencies $4.0\omega_{ci}$ and $6.0\omega_{ci}$, respectively. Thus the experimental and the simulation frequencies occur at roughly the same multiples of ω_{ci}.

As a result, assuming the magnetic waves observed by the satellites are the same ones observed in the simulations, we can identify them as magnetoacoustic waves.

CONCLUSION

We have constructed two- and three-dimensional particle fluid models inlucing the Hall term and thoroughly tested the model against theory by exploring linear wave propagation. Detailed numerical analysis of the model has been performed and thus we feel confident regarding the stability and reliability of the model. Furthermore, the model, including the Hall term, enabled us to study the nature of the waves in front of the AMPTE artificial comet and to follow the behavior over a number of ion cyclotron periods. As for future applications, numerous problems in space as well as fusion, such as ICRH, normal modes, and influence of the Hall term on instabilities, can be explored by the two- as well as three-dimensional versions of the model.

APPENDIX A: DERIVATION OF THE DISPERSION RELATION

The starting equation for the derivation of the general analytic dispersion relation of the MHD Hall term model is Eq. (26) of the analytic treatment section, i.e.,

$$-i\omega\,\delta\mathbf{B} = i\left\{\frac{\mathbf{k}\cdot\mathbf{B}_0}{4\pi\rho_0\omega}\left[\mathbf{k}(\mathbf{B}_0\cdot\delta\mathbf{B}) - \delta\mathbf{B}(\mathbf{k}\cdot\mathbf{B}_0)\right] + \frac{[(\mathbf{k}\cdot\mathbf{B}_0)(k^2c_s^2/\omega^2)\mathbf{k} - k^2\mathbf{B}_0](\mathbf{B}_0\cdot\delta\mathbf{B})}{4\pi\rho_0\omega(1-k^2c_s^2/\omega^2)}\right\} + \bar{\alpha}(\mathbf{k}\times\delta\mathbf{B})(\mathbf{k}\cdot\mathbf{B}_0), \tag{86}$$

where $\delta\mathbf{B}$ is the perturbed magnetic field, while $\mathbf{B}_0$ is the externally applied magnetic field and $\mathbf{k}$ is the wave vector.

To ease the algebra we first obtain the dispersion relation of the waves which propagate in the $x-z$ plane while the background magnetic field has an arbitrary direction specified by the polar and the azimuthal angles. Thereafter, in order to generalize this relationship to represent arbitrary propagation of the waves, i.e., to the case with $\mathbf{k} = (k_x, k_y, k_z)$, we simply make a rotation of the coordinate system in which the dispersion relation with $\mathbf{k} = (k_x, 0, k_z)$ was derived.

Let us then first consider:

$$\mathbf{k} = (k_x, 0, k_z) \tag{87}$$

$$\mathbf{B}_0 = (B_0\sin\theta\cos\varphi,\ B_0\sin\theta\sin\varphi,\ B_0\cos\theta). \tag{88}$$

The geometry is depicted in part (a) of Fig. 12. The Maxwell equation $\nabla\cdot\delta\mathbf{B} = 0$ upon Fourier transformation gives

$$\mathbf{k}\cdot\delta\mathbf{B} = 0 \Rightarrow k_x\,\delta B_x + k_z\,\delta B_z = 0 \tag{89}$$

which simply implies

$$\delta B_x = -\frac{k_z}{k_x}\,\delta B_z. \tag{90}$$

Using this along with Eqs. (87) and (88) in Eq. (86) will result in the following relationship, where the substitutions $\bar{\alpha}B_0 = c_A^2/\omega_{ci}$ and $c_A^2 = B_0^2/4\pi\rho_0$ have been made:

$$\omega^6+\omega^4\Big[-(k_x^2+k_z^2)\,c_s^2-c_A^2\sin^2\theta\cos^2\varphi(2k_x^2+k_z^2)$$
$$-2c_A^2k_xk_z\sin\theta\cos\theta\cos\varphi-c_A^2\cos^2\theta(k_x^2+2k_z^2)$$
$$-c_A^2\sin^2\theta\sin^2\varphi(k_x^2+k_z^2)$$
$$-\frac{c_A^2}{\omega_{ci}^2}\left((k_x^4+k_x^2k_z^2)\sin^2\theta\cos^2\varphi\right.$$
$$+(k_x^2k_z^2+k_z^4)\cos^2\theta$$
$$\left.+2k_xk_z(k_x^2+k_z^2)\sin\theta\cos\theta\cos\varphi\right)\Big]$$
$$+\omega^2\Big[2k_x^2(k_x^2+k_z^2)\,c_A^2c_s^2\sin^2\theta\cos^2\varphi$$
$$+4k_xk_z(k_x^2+k_z^2)\,c_A^2c_s^2\sin\theta\cos\theta\cos\varphi$$
$$+2k_z^2(k_x^2+k_z^2)\,c_s^2c_A^2\cos^2\theta$$
$$+k_x^2(k_x^2+k_z^2)\,c_A^4\sin^4\theta\cos^4\varphi$$
$$+(k_x^2+k_z^2)^2\,c_A^4\sin^2\theta\cos^2\theta\cos^2\varphi$$
$$+2(k_x^2+k_z^2)\,k_xk_zc_A^4\sin^3\theta\cos^3\varphi\cos\theta$$
$$+2(k_x^2+k_z^2)\,k_xk_zc_A^4\sin\theta\cos^3\theta\cos\varphi$$
$$+(k_x^4+k_x^2k_z^2)\,c_A^4\sin^4\theta\sin^2\varphi\cos^2\varphi$$
$$+2k_xk_z(k_x^2+k_z^2)\,c_A^4\sin^3\theta\cos\theta\sin^2\varphi\cos\varphi$$
$$+(k_x^2k_z^2+k_z^4)\,c_A^4\cos^4\theta$$
$$+(k_x^2k_z^2+k_z^4)\,c_A^4\sin^2\theta\cos^2\theta\sin^2\varphi$$
$$+\frac{c_A^4}{\omega_{ci}^2}\left((k_x^2+k_z^2)^2\,c_s^2(k_x^2\sin^2\theta\cos^2\varphi\right.$$
$$\left.+k_z^2\cos^2\theta+2k_xk_z\sin\theta\cos\theta\cos\varphi)\right]$$
$$-c_A^4k_x^4(k_x^2+k_z^2)\,c_s^2\sin^4\theta\cos^4\varphi$$
$$-6c_A^4k_x^2k_z^2(k_x^2+k_z^2)\,c_s^2\sin^2\theta\cos^2\theta\cos^2\varphi$$
$$-4c_A^4\sin^3\theta\cos^3\varphi\cos\theta(k_x^2+k_z^2)\,k_x^3k_zc_s^2$$
$$-4c_A^4c_s^2(k_x^2+k_z^2)\,k_xk_z^3\sin\theta\cos^3\theta\cos\varphi$$
$$-c_A^4c_s^2(k_x^2+k_z^2)\,k_z^4\cos^4\theta=0. \tag{91}$$

We next make a rotation of the coordinate system by an amount $-\alpha$ about the z axis as depicted in part (b) of the Fig. 12. In this new coordinate system $\varphi\to\varphi'=\varphi+\alpha$, and the wave vector $\mathbf{k}=(k_x,0,k_z)$ will change to $\mathbf{k}'$, where

$$\mathbf{k}'=\begin{pmatrix}\cos\alpha & -\sin\alpha & 0\\ \sin\alpha & \cos\alpha & 0\\ 0 & 0 & 1\end{pmatrix}\begin{pmatrix}k_x\\0\\k_z\end{pmatrix} \tag{92}$$

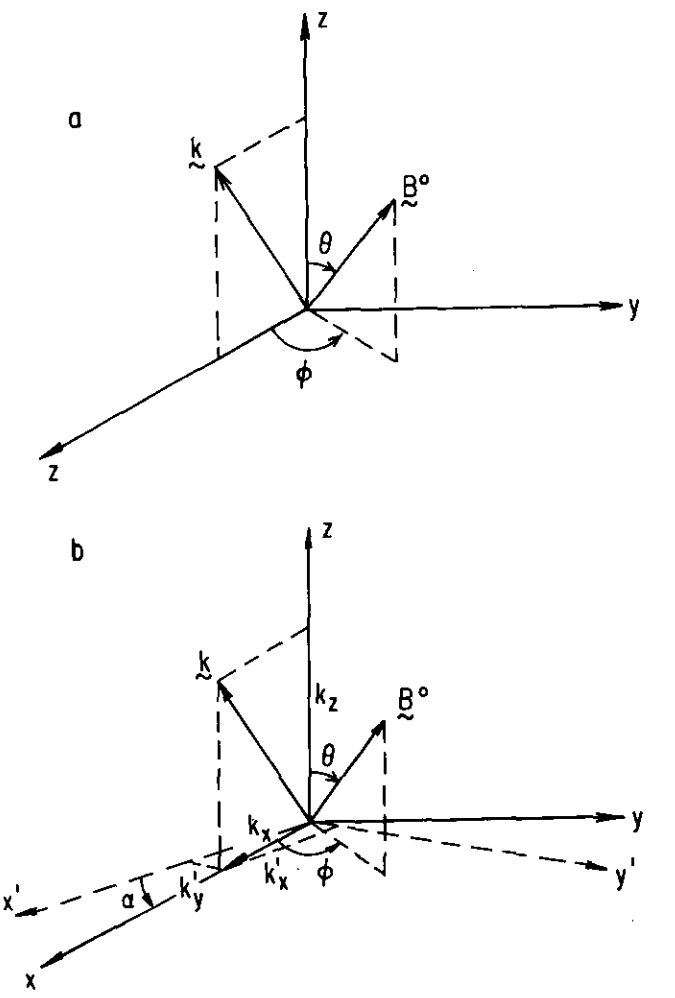

FIG. 12. (a) The geometry of the case with the waves propagating in the $x-z$ plane. (b) The geometry of the case with the waves propagating in the arbitrary direction.

from which it immediately follows that with $\mathbf{k}'=(k'_x,k'_y,k'_z)$,

$$k'_x=k_x\cos\alpha \tag{93}$$
$$k'_y=k_x\sin\alpha \tag{94}$$
$$k'_z=k_z. \tag{95}$$

Given these then it is clear that

$$\cos\alpha=\frac{k'_x}{\sqrt{k'^2_x+k'^2_y}} \tag{96}$$
$$\sin\alpha=\frac{k'_y}{\sqrt{k'^2_x+k'^2_y}} \tag{97}$$

all of these result in the simple relationships:

$$k_x=\sqrt{k'^2_x+k'^2_y} \tag{98}$$
$$k_z=k'_z. \tag{99}$$

Clearly the polar angle θ remains unchanged, while the azimuthal angle φ changes to φ', where

$$\varphi' = \varphi + \alpha. \tag{100}$$

It should then be clear that substituting for $\cos\alpha$ and $\sin\alpha$ from Eqs. (96) and (97) we obtain

$$\cos\varphi = \frac{1}{\sqrt{k_x'^2 + k_y'^2}}(k_x'\cos\varphi' + k_y'\sin\varphi') \tag{101}$$

$$\sin\varphi = \frac{1}{\sqrt{k_x'^2 + k_y'^2}}(k_x'\sin\varphi' - k_y'\cos\varphi'). \tag{102}$$

Next substituting Eqs. (98), (99), (101), and (102) with $\theta = \theta'$ in Eq. (91) will result in the general dispersion relation which we have been looking for (primes have been dropped and $k^2 = k_x^2 + k_y^2 + k_z^2$):

$$\begin{aligned}
&\omega^6 + \omega^4\Big\{-k^2c_s^2 - c_A^2\sin^2\theta[(1+\cos^2\varphi)k_x^2 \\
&\quad + (1+\sin^2\varphi)k_y^2 + k_z^2 + 2k_xk_y\sin\varphi\cos\varphi] \\
&\quad - 2c_A^2\sin\theta\cos\theta k_z(k_x\cos\varphi + k_y\sin\varphi) \\
&\quad - c_A^2\cos^2\theta(k_x^2 + k_y^2 + 2k_z^2) \\
&\quad - \frac{c_A^4k^2}{\omega_{ci}^4}[\sin^2\theta(k_x^2\cos^2\varphi + k_y^2\sin^2\varphi \\
&\quad + 2k_xk_y\sin\varphi\cos\varphi) + k_z^2\cos^2\theta \\
&\quad + 2k_z(k_x\cos\varphi + k_y\sin\varphi)\sin\theta\cos\theta]\Big\} \\
&\quad + \omega^2\Big\{k^2[2c_A^2c_s^2\sin^2\theta(k_x^2\cos^2\varphi + k_y^2\sin^2\varphi \\
&\quad + 2k_xk_y\sin\varphi\cos\varphi) \\
&\quad + 4k_z(k_x\cos\varphi + k_y\sin\varphi)c_A^2c_s^2\sin\theta\cos\theta \\
&\quad + 2k_z^2c_s^2c_A^2\cos^2\theta \\
&\quad + c_A^4\sin^2\theta(k_x^2\cos^2\varphi + k_y^2\sin^2\varphi + 2k_xk_y\sin\varphi\cos\varphi) \\
&\quad + c_A^4\sin^2\theta\cos^2\theta k_z^2 \\
&\quad + 2k_z(k_x\cos\varphi + k_y\sin\varphi)c_A^4\sin\theta\cos\theta \\
&\quad + k_z^2c_A^4\cos^4\theta] \\
&\quad + \frac{c_A^4k^4}{\omega_{ci}^2}c_s^2[\sin^2\theta(k_x^2\cos^2\varphi + k_y^2\sin^2\varphi \\
&\quad + 2k_xk_y\sin\varphi\cos\varphi) \\
&\quad + k_z^2\cos^2\theta + 2k_z(k_x\cos\varphi + k_y\sin\varphi)\sin\theta\cos\theta]\Big\} \\
&\quad + k^2\{-c_A^4c_s^2\sin^4\theta(k_x^4\cos^4\varphi + 4k_xk_y^3\cos\varphi\sin^3\varphi \\
&\quad + 4k_x^3k_y\sin\varphi\cos^3\varphi \\
&\quad + 6k_x^2k_y^2\sin^2\varphi\cos^2\varphi + k_y^4\sin^4\varphi) \\
&\quad - 6c_A^4c_s^2k_z^2\sin^2\theta\cos^2\theta(k_x^2\cos^2\varphi + k_y^2\sin^2\varphi \\
&\quad + 2k_xk_y\sin\varphi\cos\varphi) \\
&\quad - 4c_A^4c_s^2k_z\sin^3\theta\cos\theta(k_x^3\cos^3\varphi + k_y^3\sin^3\varphi \\
&\quad + 3k_x^2k_y\cos^2\varphi\sin\varphi + 3k_xk_y^2\cos\varphi\sin^2\varphi) \\
&\quad - 4c_A^4c_s^2k_z^3(k_x\cos\varphi + k_y\sin\varphi)\sin\theta\cos^3\theta \\
&\quad - c_A^4c_s^2k_z^4\cos^4\theta\} = 0.
\end{aligned} \tag{103}$$

APPENDIX B: LIST OF SYMBOLS

Symbol	Meaning
$\mathbf{r}_i$	Ion particle coordinate
$\mathbf{v}_i$	Ion particle velocity
$\mathbf{v}_f$	Fluid velocity
M_i	Proton mass
n_i	Ion number density
Π_i	Ion pressure tensor
p_i	Ion pressure
$\overline{\overline{\mathbf{I}}}$	Unit dyadic tensor
n_e	Electron number density
m_e	Electron mass
e	Electronic charge
n	Plasma number density
n_0	Background number density
ρ	Plasma mass density
T_i	Ion temperature
γ	Ratio of specific heats
c_s	$\sqrt{\gamma T_i/M_i}$ (ion acoustic speed)
$\mathbf{E}$	Electric field
$\mathbf{B}$	Magnetic field
c	Speed of light
$\tilde{\alpha}$	$c/4\pi n_0 e$ (coefficient of the Hall term)
c_A	$\sqrt{B_0^2/4\pi\rho_0}$ (Alfven speed)
$\mathbf{j}$	Electric current
$\mathbf{k}$	$(k_\parallel, \mathbf{k}_\perp)$ (wave vector)
ω	Wave frequency
ω_{ci}	Ion cyclotron frequency
ω_{ce}	Electron cyclotron frequency
ω_{pi}	Ion plasma frequency
Δ	Grid spacing
Φ	Magnetic flux
a	Particle size
Δ_g^2	Grid cell area
w	Weight function
$\mathscr{B}$	$B_z + iB_y$
g	Amplification factor
σ	$k_x\Delta$
C	Correlation function
G	Power spectrum
λ	c/ω_{pi} (skin depth)
Δt	Time step
$\mathbf{F}_B$	$n_0/n[-\nabla\cdot((B^2/2)\,\overline{\overline{\mathbf{I}}} - \mathbf{BB})]$ (magnetic force)
$\mathbf{F}_p$	$-1/n(n/n_0)^{\gamma-1}\nabla n$ (pressure force)
f	Multi-streaming coefficient

ACKNOWLEDGMENTS

This work was supported in part by the D.O.E. Contract DE-FG03-86 ER53223 and NSF Contract NSF ATM 88-18741.

REFERENCES

1. J. N. Leboeuf, T. Tajima, and J. M. Dawson, *J. Comput. Phys.* **31**, 379 (1979).
2. T. Tajima, J. N. Leboeuf, and J. M. Dawson, *J. Comput. Phys.* **38**, 237 (1980).
3. F. Brunel, J. N. Leboeuf, T. Tajima, and J. M. Dawson, *J. Comput. Phys.* **43**, 268 (1981).
4. F. Kazeminezhad, Ph.D. Dissertation, ppg-1261 (Institute of Plasma and Fusion Research, Univ. of California, Los Angeles, 1989).
5. J. Von Neumann and R. D. Richtmyer, *J. Appl. Phys.* **21**, 232 (1950).
6. C. K. Birdsall and A. B. Langdon, *Plasma Physics via Computer Simulation* (McGraw–Hill, New York, 1985), Chaps. 2, 8.
7. D. E. Potter, *Computational Physics* (Wiley, New York, 1973), Chap. 3.
8. J. M. Dawson, *Rev. Mod. Phys.* (2), 421 (1983).
9. C. Kittel, *Elementary Statistical Physics* (Wiley, New York, 1958), p. 135.
10. A. Valenzuela, G. Haerendel, H. Föppl, F. Melzner, H. Neuss, E. Rieger, J. Stöcker, O. Bauer, H. Höfner, and J. Loidl, *Nature* **320** (6064), 700 (1986).
11. D. Rees, T. J. Halliman, H. C. Stenbaeck-Nielsen, M. Mendillo, and J. Baumgardner, *Nature* **320**, (6064), 704 (1986).
12. H. Lühr, D. J. Southwood, N. Klöcker, M. W. Dunlop, W. A. C. Mier-Jedrzejowicz, R. P. Rijnbeek, M. Six, B. Häusler, and M. Acuña, *Nature* **320** (6064), 708 (1986).
13. D. J. Rodgers, A. J. Coates, A. D. Johnstone, M. F. Smith, D. A. Bryant, D. S. Hall, and C. P. Chaloner, *Nature* **320** (6064), 712 (1986).
14. L. J. C. Woolliscroft, M. P. Gough, P. J. Christiansen, A. G. Darbyshire, H. G. F. Gough, D. S. Hall, D. Jones, S. R. Jones, and A. J. Norris, *Nature* **320** (6064), 716 (1986).
15. G. Haerendel, G. Paschmann, W. Baumjohann, and C. W. Carlson, *Nature* **320** (6064), 720 (1986).
16. N. Klöcker, H. Lühr, D. J. Southwood, and M. H. Acuña, *Adv. Space Res.* **8** (1), 23 (1988) [printed in Great Britain; all rights preserved].
17. F. Kazeminezhad, R. Bingham, and J. M. Dawson, *J. Geophys. Res.*, in press (1992).